Journal of Structural Geology 108 (2018) 180–197

Contents lists available at ScienceDirect

Journal of Structural Geology

journal homepage: www.elsevier.com/locate/jsg

Implications of heterogeneous fracture distribution on reservoir quality; an analogue from the Torridon Group sandstone, Moine Thrust Belt, NW Scotland

Hannah Watkins*, David Healy, Clare E. Bond, Robert W.H. Butler

Geology and Petroleum Geology, Meston Building, University of Aberdeen, Aberdeen, AB24 3UE, Scotland, UK

ARTICLE INFO

Article history:
Received 13 December 2016
Received in revised form
30 May 2017
Accepted 1 June 2017
Available online 3 June 2017

Keywords:
Fracture
Reservoir quality
Fold-thrust belt
Tight sand
Fractured reservoir
Outcrop analogue

ABSTRACT

Understanding fracture network variation is fundamental in characterising fractured reservoirs. Simple relationships between fractures, stress and strain are commonly assumed in fold-thrust structures, inferring relatively homogeneous fracture patterns. In reality fractures are more complex, commonly appearing as heterogeneous networks at outcrop. We use the Achnashellach Culmination (NW Scotland) as an outcrop analogue to a folded tight sandstone reservoir in a thrust belt. We present fracture data is collected from four fold-thrust structures to determine how fracture connectivity, orientation, permeability anisotropy and fill vary at different structural positions. We use a 3D model of the field area, constructed using field observations and bedding data, and geomechanically restored using Move software, to determine how factors such as fold curvature and strain influence fracture variation.

Fracture patterns in the Torridon Group are consistent and predictable in high strain forelimbs, however in low strain backlimbs fracture patterns are inconsistent. Heterogeneities in fracture connectivity and orientation in low strain regions do not correspond to fluctuations in strain or fold curvature. We infer that where strain is low, other factors such as lithology have a greater control on fracture formation. Despite unpredictable fracture attributes in low strain regions, fractured reservoir quality would be highest here because fractures in high strain forelimbs are infilled with quartz. Heterogeneities in fracture attribute data on fold backlimbs mean that fractured reservoir quality and reservoir potential is difficult to predict.

1. Introduction

Fractures impact hydrocarbon reservoir quality, whether it be by increasing storage capacity and flow, creating permeability anisotropy, or by acting as impermeable barriers, thus compartmentalising the reservoir horizon or impairing flow according to fracture scale. Where primary porosity is low, such as in tight sandstone reservoirs, fractures may be crucial in providing migration pathways. To determine this, first we need to understand the controls on the formation and distribution of fractures. We present an outcrop analogue for a folded tight sandstone reservoir, using the Torridon Group sandstone, Moine Thrust Belt, NW Scotland. Natural fracture patterns are quantified and related to the larger-scale structure of folds and thrusts. This allows us to produce a general model for fracture development in these structural settings that may inform forecasts of fracture patterns and their impact on hydrocarbon production in the subsurface.

Forecasting fracture patterns has been approached in many ways. For example Price (1966) and Stearns (1969) use conceptual models to relate fracture orientation to fold geometry; both suggest up to four separate fracture sets may be found on fold structures (Fig. 1). Other studies use real-world examples to try and explain heterogeneities caused by variables such as mechanical properties of the host rock, which are not taken into account by conceptual models. These studies turn to outcrop analogues to gain insight into what controls fracture formation and variation (e.g. McQuillan, 1973; Bergbauer and Pollard, 2004; Florez-Niño et al., 2005; Wennberg et al., 2007).

Published studies that aim to determine structural and

* Corresponding author.
E-mail addresses: h.watkins@abdn.ac.uk (H. Watkins), d.healy@abdn.ac.uk (D. Healy), clare.bond@abdn.ac.uk (C.E. Bond), rob.butler@abdn.ac.uk (R.W.H. Butler).

http://dx.doi.org/10.1016/j.jsg.2017.06.002

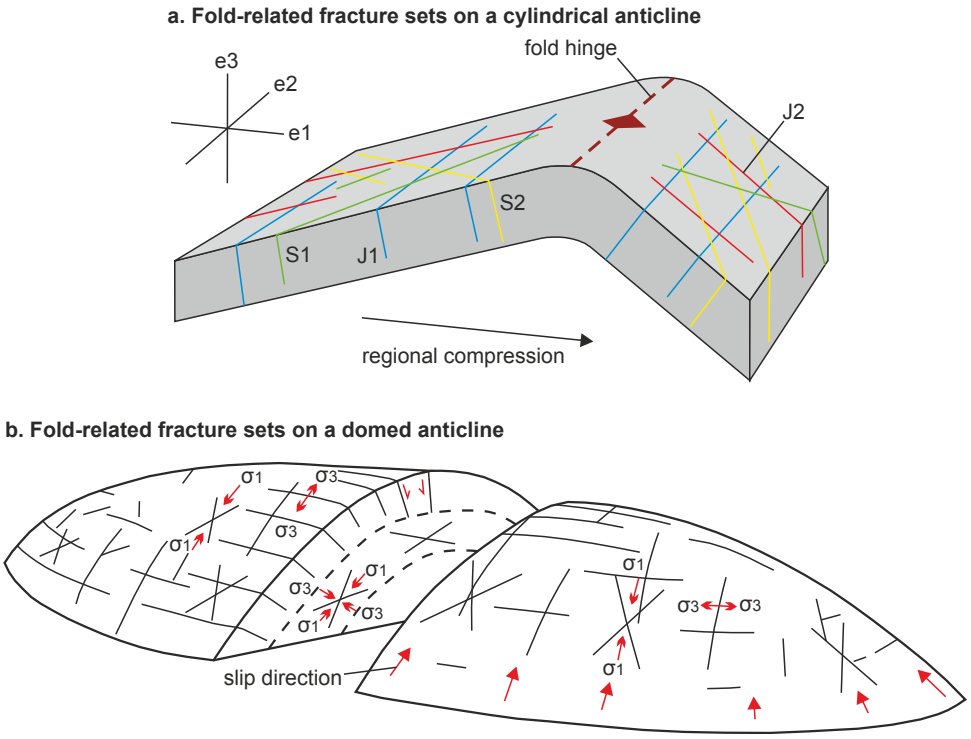

Fig. 1. a) A model of fold-related fracture sets on a cylindrical anticline: joints parallel to the fold hinge (J1), joints perpendicular to the fold hinge (J2), and conjugate shear fractures with an acute bisector parallel to regional compression and e1 (S1 and S2). Figure modified from Price (1966). b) A model of fold-related fracture sets on a dome-shaped anticline: fracture orientations vary depending on structural position/orientation of the slip direction. Figure modified from Stearns (1969).

lithological controls on fracture attributes commonly have conflicting views. Fracture density (number of fractures per unit length or unit area) and intensity (fracture length or volume per unit area or unit volume) are suggested to be controlled by the curvature of folded beds (e.g. Harris et al., 1960; Murray, 1968; Gorham et al., 1979; Lisle, 1992, 1994; Nelson and Serra, 1995; Ortega et al., 2010); by the intensity of tectonic deformation (Hobbs, 1967); strain (Nelson, 1985); or structural position on a fold (Wennberg et al., 2007; Barbier et al., 2012). Others suggest structural factors such as structural position have no influence on fracture occurrence (McQuillan, 1973; Bergbauer and Pollard, 2004), and instead fracture density and intensity is often attributed to lithological factors such as grain size (Hanks et al., 1997; Wennberg et al., 2007), porosity (Corbett et al., 1987; Barbier et al., 2012), composition (Hugman and Friedman, 1979; Corbett et al., 1987; Ferrill and Morris, 2008), clay mineral distribution (Laubach et al., 2009) and mechanical layer thickness (Hobbs, 1967; Florez-Niño et al., 2005; Wennberg et al., 2006). These lithological controls all influence the resultant mechanical stratigraphy, which is likely to change over time during diagenesis.

With a wide range of factors thought to influence fracture formation, the resultant fracture networks on a fold are likely to be complex, heterogeneous and unpredictable. An understanding of how fracture networks vary in the subsurface is important, especially if those fractures significantly affect the storage capacity and flow characteristics of hydrocarbon reservoirs. The central challenge lies in forecasting these networks using 1) determinations made from wells, 2) field data from outcrop analogues, and 3) modelling techniques. In this paper we present a fracture dataset collected in the field, which is used as a tight gas sandstone outcrop analogue for better constraining the controls on fracture formation and fractured reservoir quality in sandstone in fold-thrust belts.

2. Achnashellach Culmination

Sandstones of the Neo-Proterozoic Torridon Group of NW Scotland are established outcrop analogues for tight sandstone reservoirs in the subsurface (Ellis et al., 2012) and the region is good for studying natural fractures (Laubach and Diaz-Tushman, 2009; Hooker et al., 2011). Existing studies have focussed on the structurally simple parts of the system. Here we take the same formations into the structural complexities of the Moine Thrust Belt – specifically within the Achnashellach culmination (Fig. 2b). This area is advantageous for establishing the spatial distribution of fractures because the outcrop cover is good, with individual bedding surfaces exposed over areas of up to 20,000 m^2. Extensive outcrop coverage also means we have a good understanding of the large scale fold geometries in our field area from which we are able to construct 3D models of fold structures and compare structural geometry and 3D kinematic modelling results with fracture attribute variations to determine structural controls on fracture formation and distribution.

Folding and thrusting in the Moine Thrust Belt occurred as a result of WNW-directed compression during the Caledonian Orogeny (430-410 Ma, Mendum et al., 2009), which resulted in the movement of Moine metasediments and Lewisian basement onto the Caledonian foreland rocks of the Lewisian, the Torridon Group and overlying Eriboll and An-t-Sron Formations (Butler et al., 2007; Mendum et al., 2009). Minimum displacements of 50–100 km for the thrust belt are estimated (Elliott and Johnson, 1980; Butler, 1982; Butler and Coward, 1984), of which several tens of kilometres are thought to be accommodated by the Moine Thrust itself, due to a thick mylonite belt (Strachan et al., 2010). In the southern part of the thrust belt these displacements are located on the higher structures (Moine, Kishorn and Kinlochewe Thrusts). The Achnashellach Culmination has developed in the footwall to these higher

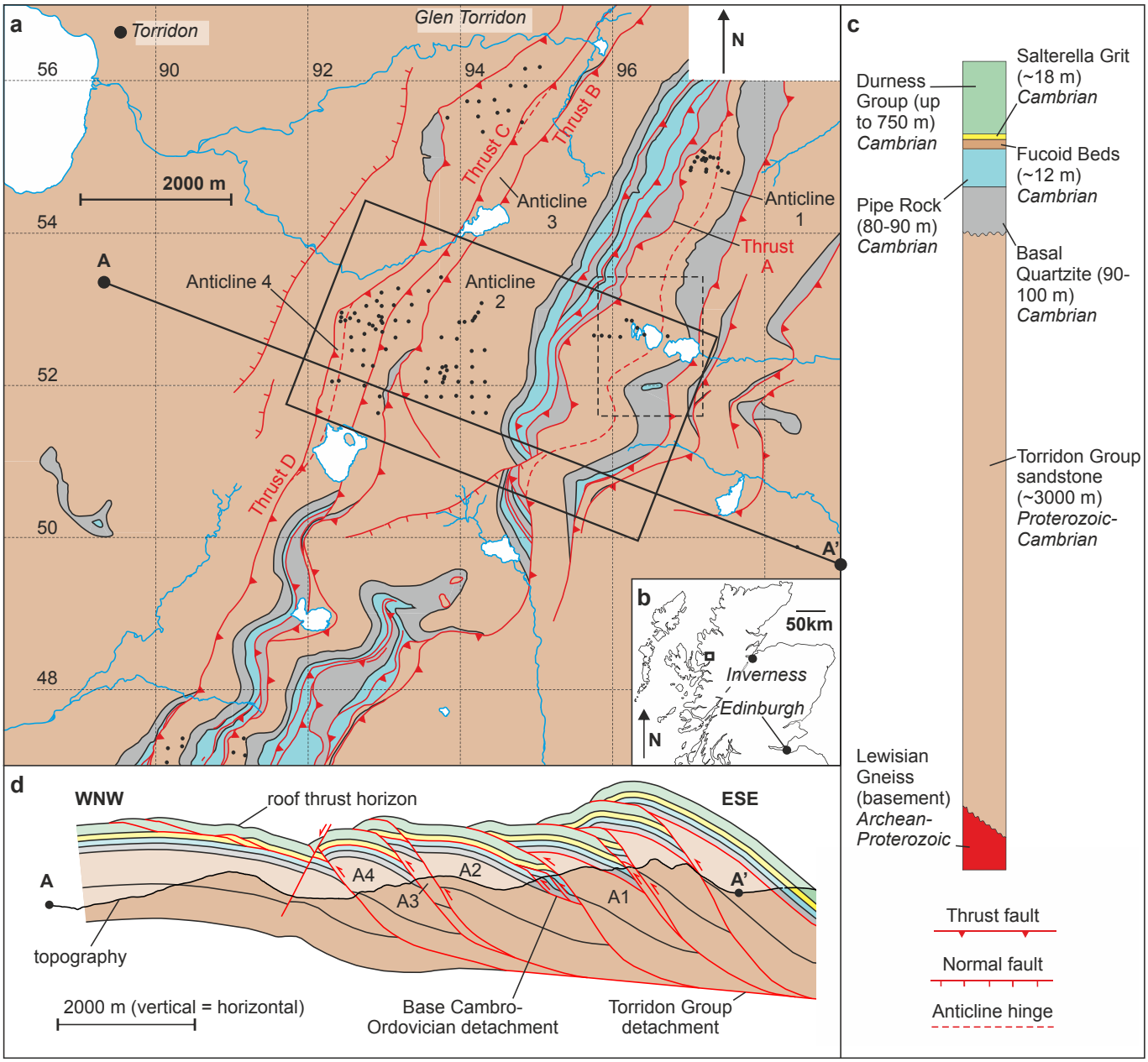

Fig. 2. a) Geological map of the Achnashellach Culmination. The black rectangle shows the extent of the 3D model (Fig. 4) and map on Fig. 10. The dashed rectangle shows the extent of the air photo on Fig. 13a. The fracture data collection points are marked as black dots. The cross section line of Fig. 2d is shown (A-A′). b) Location map of the Achnashellach Culmination (black square) in NW Scotland. c) Stratigraphic column and key to Fig. 2a, d and Fig. 10. d) Cross section A-A′ showing the fold and thrust structures of the Achnashellach Culmination, including the four anticlines studied (A1-A4). Black line within the Torridon Group is a marker horizon to show fold geometries.

thrusts and contains a ramp-dominated array of imbricates developed above the regional Sole Thrust (Butler et al., 2007). Nine of these large-scale imbricate thrusts, as well as many smaller-scale duplexes confined within the Cambro-Ordovician sedimentary rocks (Watkins et al., 2014) constitute the culmination. Exposed anticlines of the Achnashellach Culmination are primary composed of the Torridon Group and the Eriboll Formation (Fig. 2a and c). Hinges to hangingwall anticlines trend NNE, normal to the WNW transport direction for the thrust belt. Field evidence suggests that the Achnashellach Culmination formed as part of a two-stage thrust sequence. Stage 1 thrusting involved displacement on a base Cambro-Ordovician detachment (Fig. 2d), causing Cambro-Ordovician imbrication. Stage 2 thrusting involved displacement on a Torridon Group detachment (Fig. 2d), causing imbrication in the Torridon Group and Cambro-Ordovician sediments (Watkins et al., 2014). Both thrusting stages were foreland-propagating, meaning the youngest structures are to the WNW and the oldest to the ESE (Watkins et al., 2014).

The origin of sandstones of the Torridon Group is debated; some authors suggest they were deposited in a rift basin setting during the Proterozoic (1200-530 Ma; Stewart, 2002), whereas others propose they were deposited in the foreland basin to the Grenville Orogeny (Rainbird et al., 2001; Krabbendam et al., 2008). These rocks were deposited as a thick succession of cross-bedded, feldspathic fluviatile sandstones, which can be up to 5 km thick in places (Mendum et al., 2009). The Torridon Group is made up of

thick beds of coarse grained, pebbly sandstones, whose composition is quartz (45–55%); plagioclase and orthoclase (25%); illite and chlorite clays (15–20%); minor proportions of muscovite mica (Stewart, 2002). The composition of the Torridon Group makes it broadly comparable to tight gas sandstone fractured reservoirs worldwide, including the Devonian Huamampampa Formation of Bolivia and Argentina (Florez-Niño et al., 2005; Iñigo et al., 2012); the Cretaceous Williams Fork Formation of Colorado (Ozkan et al., 2009); and the Jurassic Shuixigou Group in Xinjiang Province, China (Han et al., 2016). The Torridon Group also shows very little evidence of metamorphism (Johnson et al., 1985; Van De Kamp and Leake, 1997), making it a good analogue to younger tight gas sands.

The Eriboll Formation lies unconformably on top of the Torridon Group, and consists of two quartzite members (Basal Quartzite and Pipe Rock; McClay and Coward, 1981). Above the Eriboll Formation lie the Fucoid Beds and Salterella Grit, which collectively form the An-t-Sron Formation (Swett, 1969). These units are exposed in small-scale imbricates in the southern Achnashellach Culmination.

Fracture data collection was undertaken in the Torridon Group because it is a good analogue for a folded, low-permeability (tight) sandstone. Average Torridon Group porosities within the thrust belt, measured using helium porosimetry, are 1–2%, with permeabilities ranging from 0.002 to 0.004 mD. Measured values for porosity correspond with average porosity estimates by Ellis et al. (2012) of 1.7% for the Torridon Group 40 km further north in the Moine Thrust Belt. Primary porosity and permeability are low, meaning the Torridon Group sandstone is a good analogue for a type 2 fractured reservoir, in the sense of Nelson (1985), where fractures provide the majority of permeability. Although primary porosity is low, it could still significantly improve reservoir producibility (Dutton, 1993), especially in the presence of even poorly connected fractures. Relatively few accessible outcrops of tight sandstones in fold-thrust belts are available globally. The Torridon Group sandstone could therefore be one of only a few to be used as an outcrop analogue for a folded tight sandstone gas reservoir. One limitation of the field area is outcrop coverage. Outcrops of the Torridon Group are estimated to cover only 7% of the study area (extent shown on Fig. 2a), meaning the full spatial distribution cannot be fully mapped or correlated to the full field coverage of the 3D model. This is a limitation of all outcrop studies, which should be borne in mind when deriving conclusions from field results.

In addition to compression associated with the Moine Thrust, the Torridon Group is thought to have undergone several km of burial and unloading during the Proterozoic (Ellis et al., 2012), regional tilting prior to deposition of Cambro-Ordovician sediments (Peach et al., 1907; Krabbendam and Leslie, 2010), further burial due to the emplacement of thrust sheets during the Moine Thrust events (Peach et al., 1907), post-thrusting tilting, extension and wrenching (Roberts and Holdsworth, 1999; Wilson et al., 2010), and uplift to present day exposure. Despite a complex deformation and burial history, the Torridon Group shows almost no evidence for metamorphism (Johnson et al., 1985; Van De Kamp and Leake, 1997). Torridon Group fractures are present both in the thrust belt and in the foreland to the Achnashellach Culmination. In the foreland, many fracture sets are thought to not be associated with Moine Thrust belt compression, and instead originate from other deformation and burial events that the Torridon Group has undergone (Ellis et al., 2012). Measured intensities of these fractures sets are very low (<10 m/m^2, Watkins et al., 2015b), so although it is likely that these fractures are also present in the thrust belt, the low intensity means they are unlikely to significantly impact our field results unless folding has caused their reactivation in preference to the formation of new fractures (e.g. see Guiton et al., 2003).

Fracture data collection is focussed on the four youngest fold-thrust structures in the culmination (Anticlines 1–4, see Fig. 2a). These folds formed during stage two thrusting involving the Torridon Group (Watkins et al., 2014). Fracture data collection is focussed mainly on a 4.75 × 2.7 km area in the centre of the culmination (see Fig. 2a for location), where bedding planes are well-exposed, meaning fold geometries are well constrained for 3D model building. Data is also collected from the northern and southern field area and incorporated into Figs. 6 and 9 (see Fig. 2a for data collection locations).

3. Methodology

3.1. Fracture data collection

Sampling sites were selected on Anticlines 1–4, using the workflow outlined by Watkins et al. (2015a). Initially a 200 m spacing grid square system was set up, with sampling sites located at the corners of each square. To determine small scale variations in fracture attributes, further sampling sites, spaced at 10–100 m, were selected along transects roughly parallel or perpendicular to the transport direction (see Fig. 2a for sampling locations). At each sampling site a circle of known radius (0.25–2 m) was placed on a bedding surface and the orientation of each fracture that intersects the circle was recorded, along with whether the fracture is open or mineral-filled. The number of fracture intersections with the circle (n) was noted to estimate fracture intensity using equation (1) (Fig. 3 & Mauldon et al., 2001).

$$I = n/(4r) \quad (1)$$

where I = estimated fracture intensity (m/m^2), n = number of fracture intersections with the sampling circle, and r = circle radius (m) (Mauldon et al., 2001). Estimated fracture intensity, in this case, is given as fracture length per unit area in 2D. A total of 3982 fractures were recorded from 122 sampling sites (see Fig. 2a for sampling site distribution). At each sampling circle the average grain size was recorded at outcrop, and a total of 26 samples were taken for thin section preparation to determine any lithological

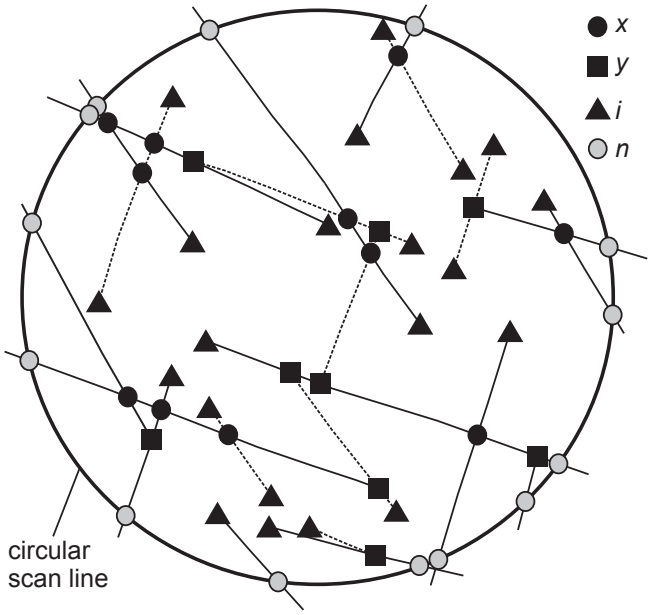

Fig. 3. Fracture intersection (Mauldon et al., 2001) and end point counting (Manzocchi, 2002) methods. 'x' points are counted where two fractures cross-cut (circles), 'y' points are counted where a fracture branches off, or abuts against a neighbouring fracture (squares), and '*I*' points are counted where a fracture tip is isolated (triangles). n points are counted where a fracture intersects the circle.

controls on fracture attributes.

Each sampling circle was also photographed for fracture trace map creation, and samples were taken from selected outcrops. 2D fracture connectivity was calculated from field photographs by counting fracture end points and intersections within each sampling circle (Fig. 3). An '*x*' node was counted when two fractures crossed one another, a '*y*' node was counted when a fracture branched off or abutted against another and an '*i*' node was counted when a fracture tip was isolated (Manzocchi, 2002). More '*x*' and '*y*' nodes means a higher fracture connectivity. The number of '*x*' and '*y*' nodes per square metre is calculated for each sampling circle area, and used as a proxy for 2D fracture connectivity, hereafter termed C_{xy}. Both cemented and open fractures are used to calculate 2D fracture connectivity rather than only open fractures; the origin of cement may be specific to this field area meaning the fracture cement distribution would not be applicable to other fractured sandstone folds. Therefore to provide an outcrop analogue study, the connectivity of all fractures should be calculated.

Field photographs are also used to estimate 2D permeability anisotropy using a tensorial approach. Fracture trace maps, created from field photographs, are used to estimate 2D permeability tensors using FracPaQ (Healy et al., 2016) and based on equations in Oda (1986), Oda and Hatsuyama, (1987) and Brown and Bruhn (1998). Fracture orientations, lengths and spatial density are taken into account, and the fracture aperture is assumed constant (0.25 mm) in this plate-parallel model of fluid flow. This approach is used to give an upper estimate for permeability anisotropy assuming all fractures are conductive. We are not attempting to model permeability so actual values for fracture aperture are not required. The magnitude of inferred permeability anisotropy (i.e. the k_1:k_2 ratio) and the orientation of maximum permeability (k_1) in 2D on the bedding surface are calculated. Permeability ellipses are shown scaled with their semi-axes equal to $\sqrt{k_1}$ and $\sqrt{k_2}$ to illustrate the anisotropy in the direction of flow (Long et al., 1982). The majority of fractures are normal to bedding, and therefore the maximum permeability is likely to be parallel to these fractures. However, few bed cross-section exposures are available to constrain permeability anisotropy in 3D, therefore 2D permeability anisotropy calculated from bedding surfaces was the focus of this study.

3.2. 3D model building

To determine structural controls on fractured reservoir attributes, a 3D model of the 4 sampled anticlines was generated in Move software (Midland Valley Exploration Ltd., 2013, 2014) using bedding data and field observations (see Watkins et al., 2014; Watkins, 2015 for a detailed model building workflow). Move was then used to restore surfaces and calculate strain distributions for each structure. The results of this 3D model building and restoration were compared with field fracture data to determine structural controls on fracture attribute variation.

The first stage of the model building process was to create ten parallel, closely-spaced cross sections in the area of interest. The cross sections cover an area of 4.75 × 2.7 km on Anticlines 1–4 (see Fig. 2a). Within this area, bedding plane exposure of the Torridon Group sandstone is good, meaning bedding orientations are well-constrained. These cross sections are spaced 300 m apart, and oriented at 110–290°. The orientation of the cross sections was calculated by determining the normal to average bedding strike for Torridon Group, Basal Quartzite and Pipe Rock. This orientation is parallel to the regional transport direction (WNW). Torridon Group bedding data within 150 m of individual cross section traces was projected onto each cross section and used to construct the top Torridon Group horizon. Thrust geometries were determined from field photographs and sketches, where good vertical sections exposed several hundred metres of thrusts. Once thrusts and top Torridon Group horizon lines for Anticlines 1–4 had been created on each section line, 3D surfaces were generated for the Top Torridon Group surface. Surfaces were smoothed and resampled to ensure fold and thrust geometries were geologically realistic. Surfaces were initially resampled to generate a maximum edge length of 100 m for each mesh triangle. Meshes were then double sampled, meaning the resultant mesh triangles have edge lengths of 30–50 m. This mesh size gives a Top Torridon surface comprising of 4034 triangles for Anticline 1, 14,696 triangles for Anticline 2, 5242 triangles for Anticline 3 and 3244 triangles for Anticline 4.

3.3. Strain modelling

Once a geologically realistic 3D model for the top Torridon Group horizon of Anticlines 1–4, and Thrusts A-D had been created from field data, fold surfaces were restored to calculate strain associated with folding and thrusting. For each fold and thrust pair, restoration was undertaken in two stages. Initially fault displacement was restored using a fault parallel flow algorithm. 2D forward modelling by Watkins et al. (2015b) showed that fault parallel flow is the most appropriate thrusting mechanism because this mechanism, along with trishear, was found to be the best at recreating fold geometries of the Achnashellach Culmination in 2D. This was followed by unfolding using geomechanical modelling. The geomechanical modelling in Move uses a mass-spring algorithm (Provot, 1995) to reduce strain whilst maintaining the original surface shape (Shackleton et al., 2009). The mesh surface acts as a network of springs, each with a certain stiffness (Bond et al., 2013), and the mechanical properties of the surfaces depend on the elastic properties of the rock. For this modelling we used the mechanical properties of sandstone with density 2500 kg/m^3, Young's modulus 15 GPa and Poisson's ratio 0.295. These are the default values for sandstone (Berea Sandstone) given in Move software and have not been calculated specifically for Torridon Group sandstones. Since Anticlines 2 and 3 are nearly planar in their present day state, only a minimal amount of unfolding by geomechanical modelling was required after fault parallel flow restoration. Following fault parallel flow restoration, Anticlines 1 and 4 still showed high curvature geometries, so significant unfolding by geomechanical modelling was required to flatten the remaining surface topography.

A 2 stage-restoration approach was chosen because no other method could be found to sufficiently restore fault displacement and unfold surfaces using a single restoration algorithm, without causing significant area change. Although this two-stage restoration is able to restore fold geometries, it is not a very realistic approach to fault and fold restoration because, in reality, folding and thrusting occurs synchronously. The two-stage restoration used is a result of modelling limitations; it is not suggested that deformation actually occurred by separate faulting and folding events. Although the approach used may not be entirely realistic, the resulting strain distributions (see Fig. 4b) follow expected patterns: high strains are found in high curvature regions and low strains are found in low curvature regions.

From the restoration process, strain was calculated for each mesh surface triangle on each fold structure. Each triangle in the mesh surface is assigned a single value for strain; a greater number of triangles (i.e. smaller mesh size) means higher strain resolution. From the restored state, forward modelled strain can be calculated from unfolded to folded states. Because a two-stage restoration was used, strain was calculated separately for fault parallel flow and geomechanical modelling. These strains are combined in the forward modelling strain calculation, firstly by calculating forward modelled folding related strains (geomechanical modelling), then

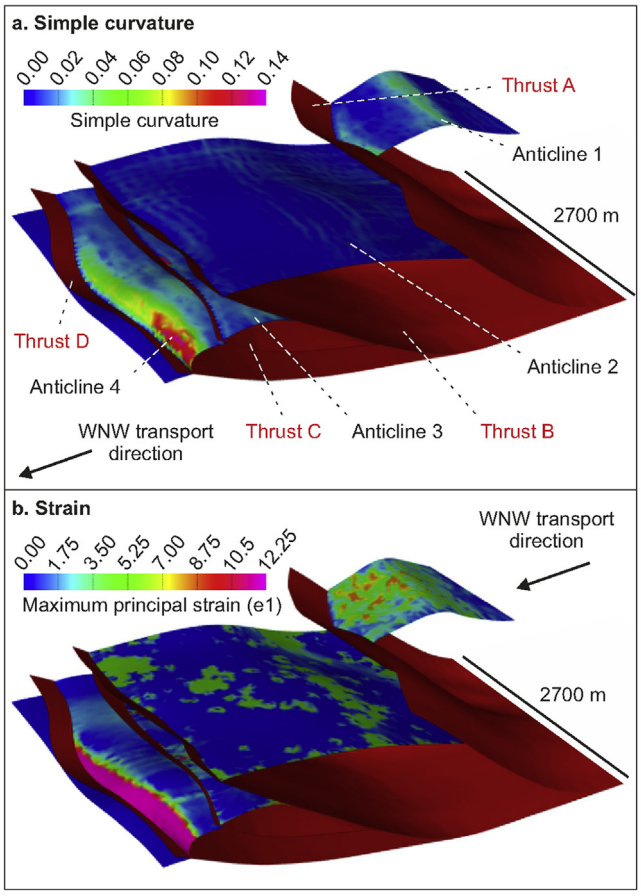

Fig. 4. a) 3D model of the Top Torridon Group horizon in the central Achnashellach Culmination, colour-mapped for simple curvature. b) 3D model of the Top Torridon Group horizon in the central Achnashellach Culmination, colour-mapped for maximum principal strain (e1), calculated by restoring fold surfaces using Move software. The extent of the 3D models is shown on Fig. 2a. A curvature and a strain value is computed for each individual triangular component of the mesh surfaces, which have edge lengths ranging from 30 to 50 m. (For interpretation of the references to colour in this figure legend, the reader is referred to the web version of this article.)

adding on forward modelled thrusting related strains (fault parallel flow).

The method used for calculating strain relies on multiple inputs, which are uncertain. The basic data used to construct cross sections, from which the 3D model is built, is bedding data collected in the field. This data was collected using a conventional compass-clinometer; small errors in dip and strike measurements for bedding surfaces are possible, however they are not large enough to alter the interpreted large-scale fold geometries. Uncertainty in interpretation associated with cross section construction makes such measuring errors limited in their overall impact. At the 3D model creation stage the main source of uncertainty, in our opinion, comes from 3D surface construction; smoothing and resampling of surfaces is completed in the software to remove kinked geometries associated with the model building process. This is a standard workflow, but may smooth true geological heterogeneity. The restoration process probably introduces uncertainty due to the two-stage method used, as previously discussed. This might impact the values for total strain, although the strain distribution should be largely unaffected. It is important to be aware of uncertainty accumulated into strain calculations from the interpretation and model building process. Although, beyond the scope of this paper, future work could investigate the impact of the different input and workflow elements on strain modelling outcome and fracture prediction.

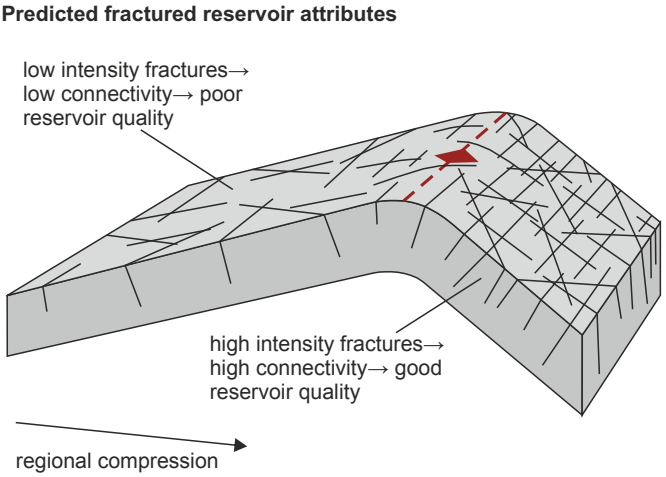

Fig. 5. Predicted fractured reservoir attributes on an anticline. Fracture orientations are based on Price (1966) model (Fig. 1a), and fracture intensity and connectivity is predicted using modelled 3D strain distribution (Fig. 4b).

4. Results: 3D model & fracture predictions

Fig. 4a shows a 3D model of the top Torridon Group horizon for Anticlines 1–4, within the study area (see black box, Fig. 2a, for location). The 3D model is colour-mapped for simple curvature (the rate of change of dip measured in the direction of maximum dip (e.g. Hennings et al., 2000)), and highlights the variations in fold geometries. Anticline 1 is the oldest structure, and shows a narrow, moderate curvature hinge and straight limbs. Anticline 2 has very low curvature, as does Anticline 3. Anticline 4 exhibits a low curvature backlimb and a very high curvature forelimb, where bedding is commonly steep and, in some places, overturned. Fig. 4b shows strain for combined fault and fold restorations on Anticlines 1–4. In general strain corresponds to fold curvature (Fig. 4a). Where curvature is highest, on the forelimb of Anticline 4, a zone of high strain is seen. In low curvature regions, such as the backlimbs of Anticlines 2–4, strain is generally low. Anticline 1 is an exception to this trend because modelled strain is moderate to high on fold limbs, whereas limb curvature is generally quite low. This is because Anticline 1 has accumulated strain during the formation of the underlying folds (Anticlines 2–4), as well as during initial slip on Thrust A, as shown by the modelling process. Anticline 2 does not show evidence for strain accumulation during the formation of younger structures, probably because low displacement on thrust D associated with the formation of Anticline 4, did not produce significant uplift of overlying folds in the 3D model restoration. The 3D model shows the relative sizes of each anticline studied; they vary in size, with Anticline 2 being the largest an Anticline 3 being the smallest. It may be difficult to draw conclusions, especially from Anticline 3, since it is so small and only a few sampling sites are located on this structure.

Based on relationships between curvature/strain and fracture attributes reported in the literature, along with our 3D model estimates for strain distribution on Anticlines 1–4, we can begin to predict how fracture attributes might vary at different structural positions in the Achnashellach Culmination. Price (1966) suggested we might expect to find 4 sets of fractures with different orientations on a thrust-related anticline (Fig. 1). Nelson (1985) suggests the intensity of fractures increases with the increasing strain. Based

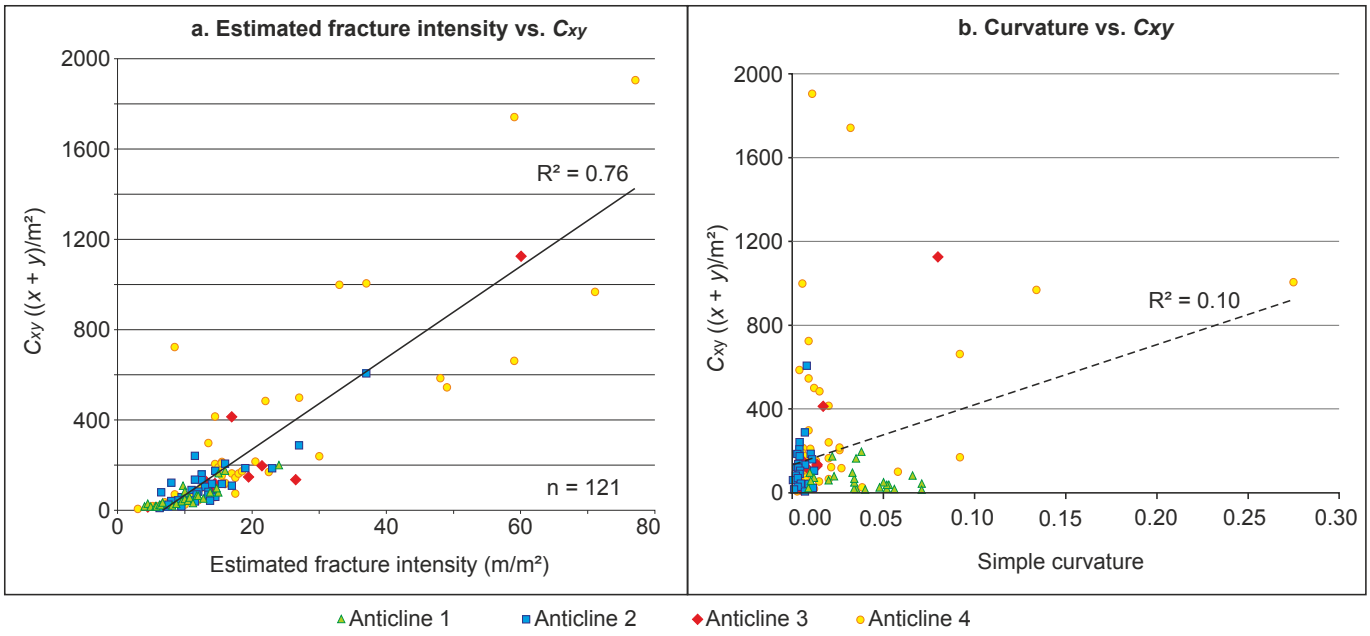

Fig. 6. a) Scatter graph of estimated fracture intensity versus 2D connectivity (C_{xy}) at each sampling site. A good correlation ($R^2 = 0.76$) suggests that estimated fracture intensity exerts a control on fracture connectivity. b) Scatter graph of fold simple curvature versus 2D fracture connectivity (C_{xy}) at each sampling site. A poor correlation is evident; significant data scatter suggests factors other than fold curvature control fracture connectivity.

on these relationships we predict to find four main fracture sets (J1, J2, S1 & S2), as outlined by Price (1966) whose estimated intensity is highest in high strain regions (i.e. the forelimbs of Anticline 1 & Anticline 4), and lowest in low strain regions (i.e. Anticline 2, Anticline 3, and the backlimbs of Anticlines 1 & 4) (Fig. 5). Fracture intensity may influence fracture connectivity; the higher the estimated intensity (i.e. fracture length per unit area), the more chances of individual fractures intersecting in a given area. This depends on the lengths of fractures and assumes fractures are at different orientations (because perfectly parallel fractures cannot intersect one another). Assuming fractures in the Torridon Group are long enough to intersect and are at variable orientations we predict fracture connectivity will be influenced by fracture intensity, and will therefore also be higher in high strain regions and lower in low strain regions. Although we can predict strain and, from this, fracture distribution on a large scale, fracture variation on a smaller scale than the size of the surface mesh triangles may not be possible to forecast.

5. Results: field data

5.1. Connectivity

Fracture connectivity can be an important factor that affects fractured reservoir quality, especially in type 2 reservoirs where fractures enhance the permeability. In theory, fracture connectivity increases with increasing fracture intensity due to more fracture intersections, provided fractures are oriented so as to allow for fracture intersection to occur (i.e. not parallel). 2D estimated fracture intensity and connectivity (C_{xy}) were calculated for each sampling site within the field area, and plotted on a scatter graph (Fig. 6a). A good correlation is found between the two variables (least squares regression, coefficient of determination $R^2 = 0.76$), indicating that fracture connectivity is, at least partially, controlled by fracture intensity.

Based on our predictions for fracture attribute variation (section 4), we would expect to find fracture connectivity increasing with increasing strain and curvature. A graph of 2D connectivity (C_{xy}) versus simple curvature (Fig. 6b) for the four anticlines sampled shows a very weak positive correlation between the two variables ($R^2 = 0.10$). As curvature increases, connectivity increases, however the data shows significant scatter. To determine why such variability in fracture connectivity is observed, we must look at the connectivity distribution on individual structures. Fig. 7a and c shows 2D connectivity (C_{xy}) contour maps for Anticlines 2 and 4 in the central part of the study area (see Fig. 2a). Anticline 4 shows a band of high fracture connectivity in the forelimb, running parallel to the fold hinge. Fracture connectivity is generally higher in the forelimb than the backlimb for this structure. These connectivity patterns correspond to predicted strain in the 3D model (Fig. 7b), suggesting that strain does, at least in part, influence connectivity. However, anomalies to this pattern are seen on the backlimb. Fig. 7a shows points of elevated fracture connectivity that do not correspond to any strain variations (Fig. 7b). The same observation is made on Anticline 2 (Fig. 7c), where an isolated connectivity anomaly is seen in a low strain backlimb region (Fig. 7d). The value of fracture connectivity at this anomaly is approaching connectivity values seen in the forelimb of Anticline 4, where strains are calculated to be 5–7 times higher than on Anticline 2. These observations indicate fracture connectivity may be partially influenced by factors other than strain in these backlimb regions.

5.2. Orientation

Fracture orientation is important because it is likely to affect permeability anisotropy in fractured reservoirs. For example if only one dominant fracture orientation is present, fracture permeability is likely to be parallel to those fractures, and therefore strongly anisotropic. Rose plots for fracture orientation are shown for a selected number of representative sampling sites on Fig. 8. The high strain forelimb of Anticline 4 (Fig. 8a) exhibits a dominant, hinge parallel joint set (J1) that is consistent across a large area. These fractures form as a result of localised WNW-ESE outer arc extension during folding. A strike-parallel transect on the backlimb of

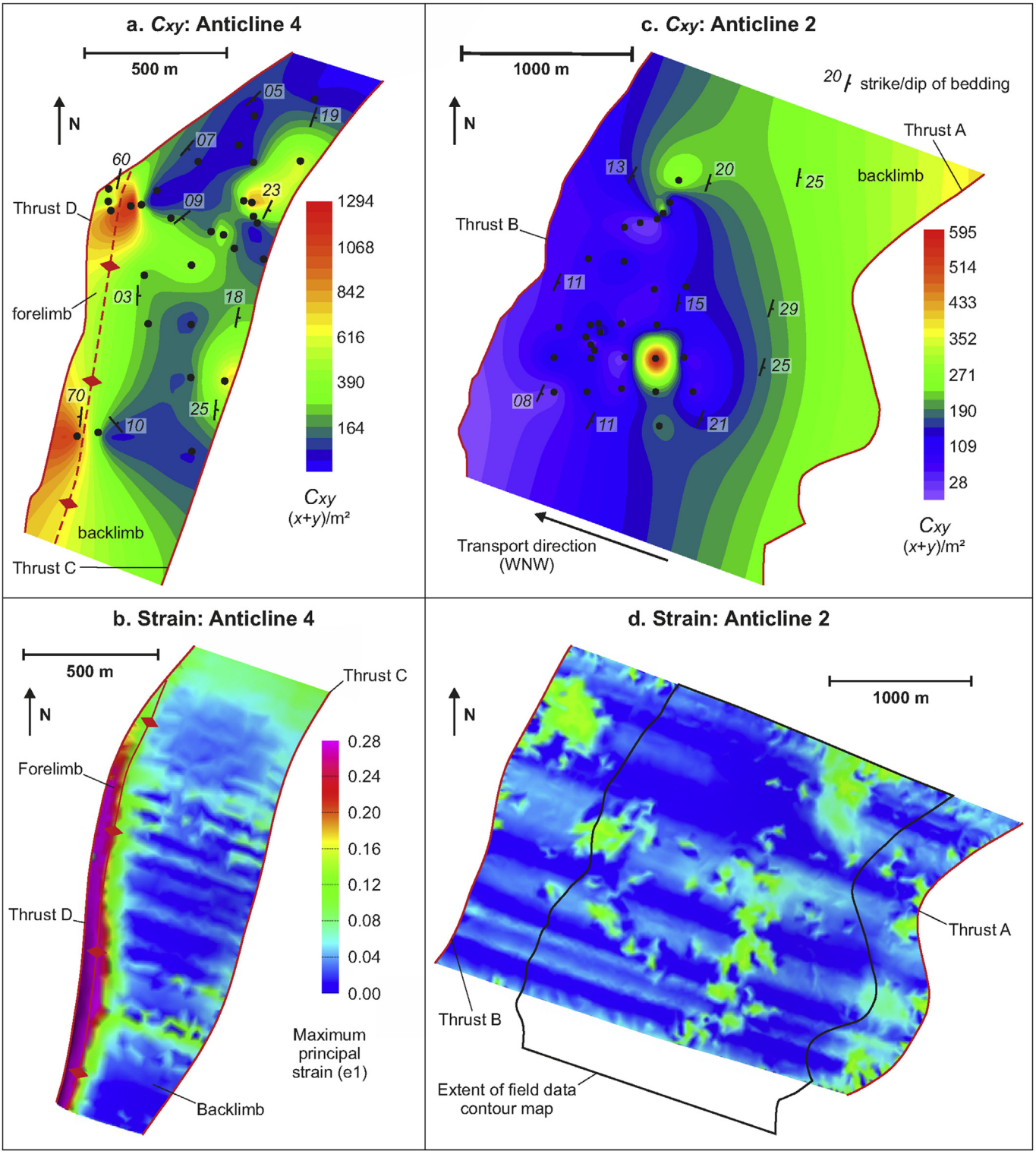

Fig. 7. a) Contour map of 2D connectivity (C_{xy}) for field data on Anticline 4. Contours generated using a least curvature method. Connectivity is consistently high in the forelimb, and lower and more variable in the backlimb. b) Strain on Anticline 4, calculated using 3D surface restoration in Move. Strain is high in the forelimb and low on the back-limb. c) Contour map of 2D connectivity (C_{xy}) for field data on Anticline 2. Contours generated using a least curvature method. Connectivity is generally low, with anomalies that do not correlate to strain. d) Strain on Anticline 2, calculated using 3D surface restoration in Move. Strain is generally low, with minor fluctuations. Linear strain trends in b and d, oriented WNW-ESE, are an artefact of fault parallel flow restoration and do not reflect true strain distributions.

Anticline 4 (Transect 1, Fig. 8b, transect location on Fig. 10a) shows fracture orientations can vary significantly over short distances in low strain regions. Sites 1 and 3 each show a single dominant fracture orientation, although the modal orientation of these is not the same. Sites 4 and 5 both show two main fracture sets, but again the orientation of these sets do not correspond, despite the

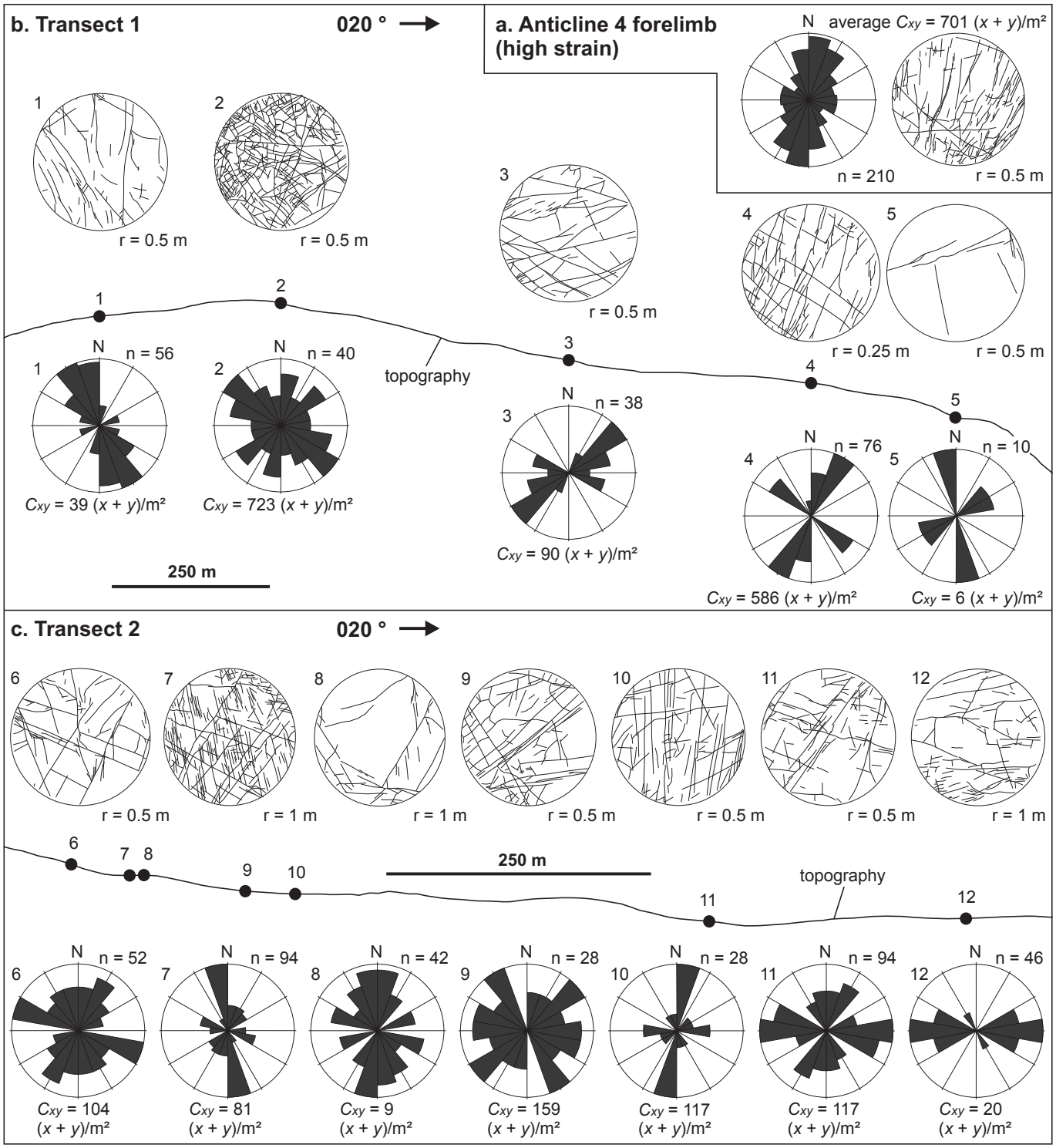

Fig. 8. a) Rose plot showing fracture orientations at all sampling sites in the high strain forelimb of Anticline 4 (left) and fracture trace map of one representative sampling site in this region (right). Fractures are dominantly oriented NNE-SSW, parallel to the fold hinge and are quartz-filled. An average connectivity value for this region is given (Cxy = 701 intersection points per square metre). b) Fracture orientations and trace maps along a strike-parallel line (Transect 1, see Fig. 10a for location). c) Fracture orientations and trace maps along a strike-parallel line (Transect 2, see Fig. 10a for location). Both transects show fracture orientation (rose plots), connectivity (c values) and distribution (fracture trace maps) can vary over short distances in these low strain back-limb locations. Fracture along these transects are open and do not contain quartz cement at outcrop. Rose plots are area-scaled; the outer ring represents a value of n. For all figures number of fractures, r = circle radius.

sampling sites being located only 250 m apart. Site 2 shows no dominant fracture sets, instead fracture orientations are dispersed. Transect 2 (Fig. 8c) is a strike parallel line on the backlimb of Anticline 2 and also shows significant variations in fracture patterns between adjacent sampling sites. For example, sites 7 and 8 exhibit different orientation distributions, despite being only 20 m apart, and on the same bedding surface.

As well as analysing fracture orientation variation on small-scale

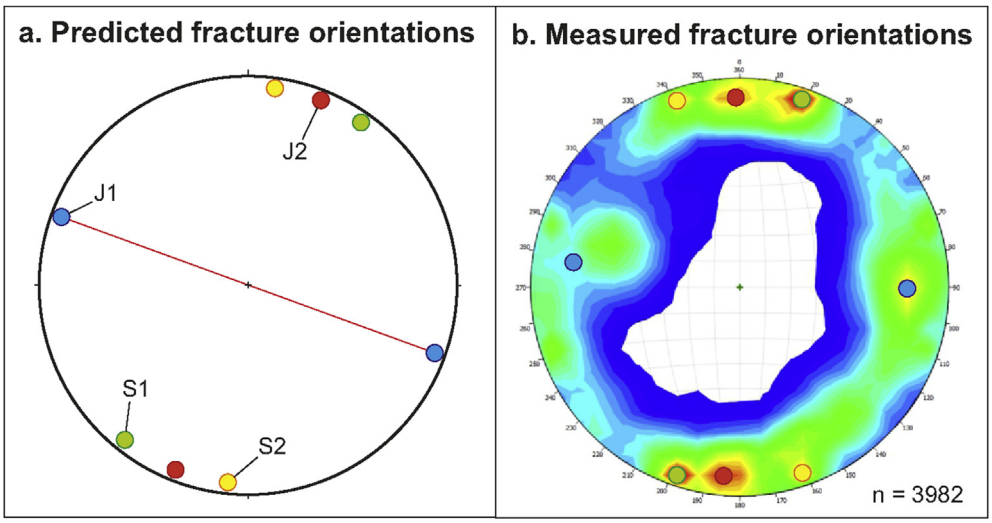

Fig. 9. a) Schematic stereonet showing the expected positions of fracture set clusters based on the fold-fracture model by Price (1966), Fig. 1a, and the estimated thrust transport direction for the Achnashellach Culmination (line). J1 are joints parallel to the fold hinge; J2 are joints parallel to the thrust transport direction; S1 and S2 are conjugate shear fractures with an acute bisector parallel to the thrust transport direction. b) Equal area stereonet showing contoured poles to fracture planes for fractures measured at all sampling sites, following structural dip removal. Fracture cluster centres, estimated using a k-means clustering algorithm (Hartigan and Wong, 1979) in Move, are shown. A contour interval of 0.2% is used.

transects, data for all sampling sites within the field area (Fig. 9) were used to determine whether significant variation could be found on a large-scale. Using the thrust-related fracture orientation model proposed by Price (1966), along with our estimated thrust transport direction for the study area (110–290°), a schematic stereonet showing the expected locations of pole to fracture plane clusters was constructed (Fig. 9a). Poles to fracture planes for all sampling sites within the study area are plotted and contoured following structural dip removal to show orientation distribution on Fig. 9b. Eight orientation cluster centres have been calculated using a k-means clustering algorithm (Hartigan and Wong, 1979) in Move; these are plotted on Fig. 9b.

The relative positions of these cluster centres clearly replicate the pattern on the schematic stereonet (Fig. 9a), although the exact orientations appear to be rotated anticlockwise by roughly 20°. These observations suggest that although fracture orientations appear highly variable and unpredictable on a small scale (see Fig. 8b and c), there is a much clearer pattern to their distribution on a large scale. According to Price (1966), the J2 fracture set should be orientated parallel to the thrust transport direction. The strike of our J2 fracture set on Fig. 9b trends E-W, indicating an E-W transport direction. However, the transport direction calculated using the average bedding dip direction for bedding data is ESE-WNW. This difference is probably because the average dip direction was calculated from Torridon Group, Basal Quartzite and Pipe-Rock outcrops. An unconformity between the Torridon Group and the overlying Basal Quartzite means they are not parallel, therefore the calculated average dip direction is not necessarily parallel to thrust transport direction.

5.3. Permeability anisotropy

2D permeability anisotropy on bedding surfaces is inferred from the orientations, densities and lengths of fractures in a network. Permeability anisotropy is analysed from fracture trace maps at each sampling site, and a representative sample is presented. Sampling sites in the high strain forelimb of Anticline 4 (site 1, Fig. 10a) consistently show strong inferred permeability anisotropy (k_1:k_2 6.46) NNE-SSW, parallel to the fold hinge. This is because fracture orientations are unidirectional, and mostly oriented parallel to the hinge (see Fig. 8a). In the backlimb of Anticline 4, variable fracture orientation distributions mean inferred permeability anisotropy varies. In some cases sampling sites show strong anisotropy (e.g. site 2, Fig. 10a, k_1:k_2 2.95) due to only one dominant fracture orientation. In other cases multiple fracture orientations mean 2D permeability is inferred to be almost isotropic, for example site 3 (k_1:k_2 1.09, Fig. 10a). No dominant orientation for permeability is seen on the backlimb of Anticline 4 (Fig. 10b) because fracture orientations are so dispersed.

Sampling sites on Anticline 3 are all in backlimb positions. Inferred permeability anisotropy varies (k_1:k_2 1.41–4.84, Fig. 10a), however the permeability orientation is consistently W-E/WNW-ESE (Fig. 10b). This indicates fracture permeability may be accommodated by well-developed J2 fractures, oriented perpendicular to fold hinges. Sampling sites on Anticline 2 are also all in backlimb positions. Inferred permeability anisotropy varies (k_1:k_2 1.06–2.89, Fig. 10a), as does the orientation of maximum permeability (Fig. 10b). A variation in magnitude of anisotropy is caused by the difference in orientation distributions at sampling sites. Some sites have a single dominant fracture orientation, which gives strong anisotropy (sites 8 & 9, Fig. 10a), whereas some sites have dispersed fracture orientations, leading to weak anisotropy (sites 6, 7 & 10, Fig. 10a). This orientation dispersion means no dominant orientation of maximum permeability is seen on this structure (Fig. 10b).

Anticline 1 generally exhibits two orthogonal fracture sets (Fig. 10a, site 12). Moderate anisotropy is usually observed (k_1:k_2 2.69 & 3.22, sites 11 & 12), and the orientation of maximum permeability is usually parallel to one of these fracture sets (NW-SE or NE-SW, Fig. 10b). In high strain regions, permeability is moderately-strongly anisotropic, and the orientation of maximum permeability is either parallel or perpendicular to fold hinges. In low strain regions, inferred permeability anisotropy is much more variable and the orientation of maximum permeability does not necessarily relate to the fold structures. This is because fracture orientations are dispersed.

5.4. Fracture fill

Hinge-parallel fractures in the forelimb of Anticline 4 (J1) are consistently quartz-filled (93% of sampled fractures), with

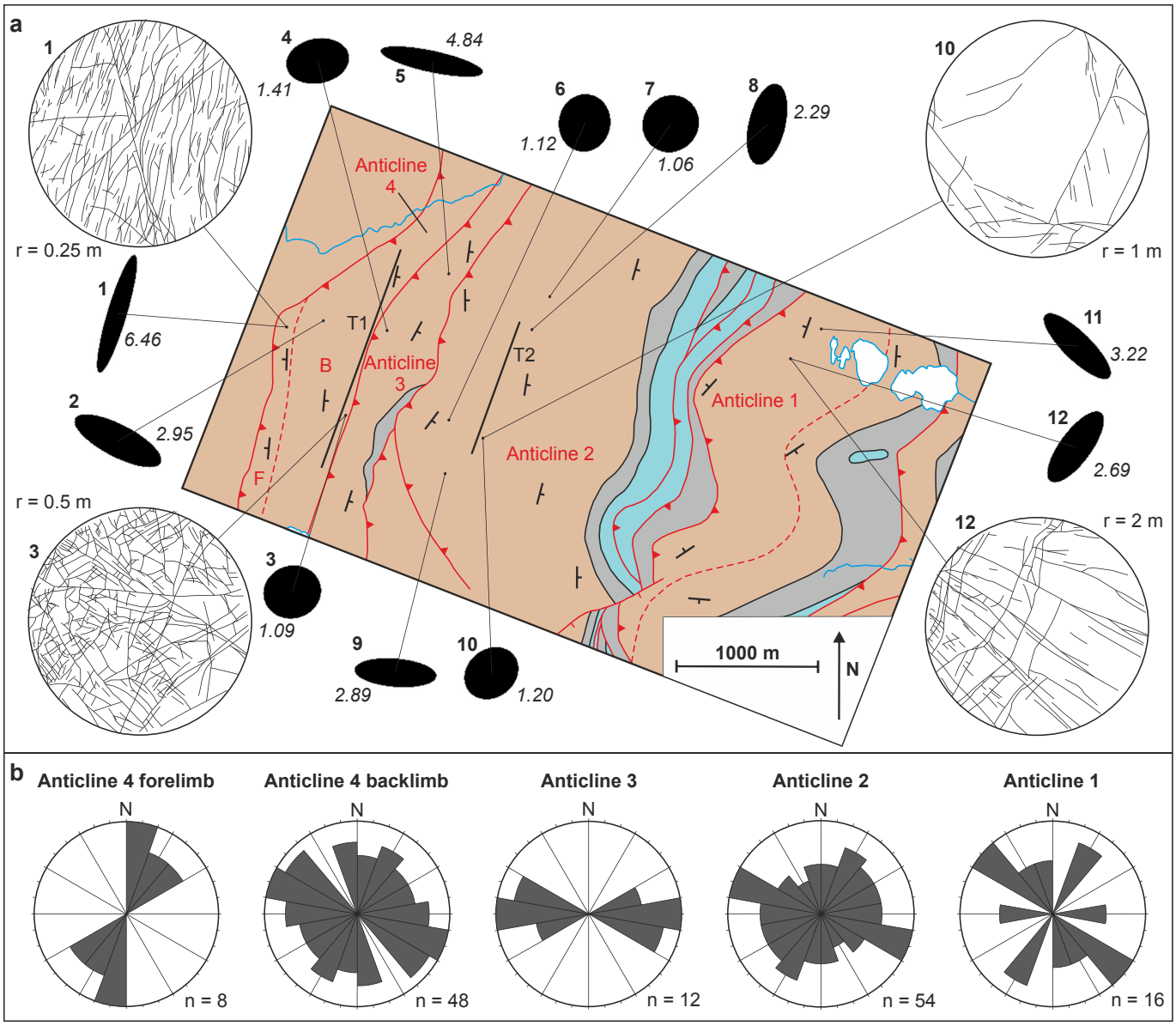

Fig. 10. a) Fracture trace maps and 2D permeability ellipses for selected sampling sites in the central Achnashellach Culmination (see Fig. 2a for map extent). Ellipse ratios represent the degree of anisotropy (k_1:k_2 for each site is shown in italics) and the orientation of ellipse long axes represent the orientation of maximum permeability, k_1. b) Rose plots showing the orientations of maximum permeability for all sampling sites on Anticlines 1–4. In the high strain forelimb of Anticline 4, the orientation of maximum permeability is NNE-SSW, parallel to the fold hinge and J1 fractures. In the moderate strain hinges of Anticline 1, the orientation of maximum permeability is usually either NE-SW or NW-SE, parallel to J1 or J2 fractures. In the low strain back-limb regions, the orientations of maximum permeability are dispersed due to dispersed fracture orientations. An exception is Anticline 3 where permeability anisotropy appears to be controlled by J2 fractures. Rose plots are area-scaled.

apertures ranging from 0.5 to 13 mm (average 1.12 mm, 1.49 standard deviation) (Fig. 11a). This means there is little remaining secondary porosity and permeability in this region, except for low estimated intensity, long fractures that sometimes remain open (see Fig. 11a). Thin sections from the forelimb of Anticline 4 show matrix grains are closely-packed, commonly forming convex and concave boundaries between adjacent quartz grains, which might indicate chemical dissolution (Fig. 11b).

The majority of fractures on Anticlines 1, 2, 3 and the backlimb of Anticline 4 are open at outcrop (83.71%) (Fig. 11c); no fracture cement is observed but may have once been present on fracture walls and subsequently removed by erosion. Open fractures could potentially provide significant porosity and permeability if they remain open, although an exact calculation of fracture porosity has not been made because fractures are weathered at outcrop meaning actual aperture measurements are inaccurate. Fractures in tight gas sandstones have been shown be relatively stiff and to remain open at great depth (as much as 6000 m) in any orientation relative to current day stress orientation (Laubach et al., 2004, 2016). The open fractures we found may be representative of subsurface arrays. Thin sections from these backlimb regions (Fig. 11d) show grains are not as closely-packed as in the forelimb of Anticline 4 (Fig. 11b). Instead most matrix grains are coated in a thin mud and clay lining, meaning there is little contact between neighbouring grains.

6. Discussion

6.1. Fracture heterogeneity

Analysis of fracture data collected in the Torridon Group from

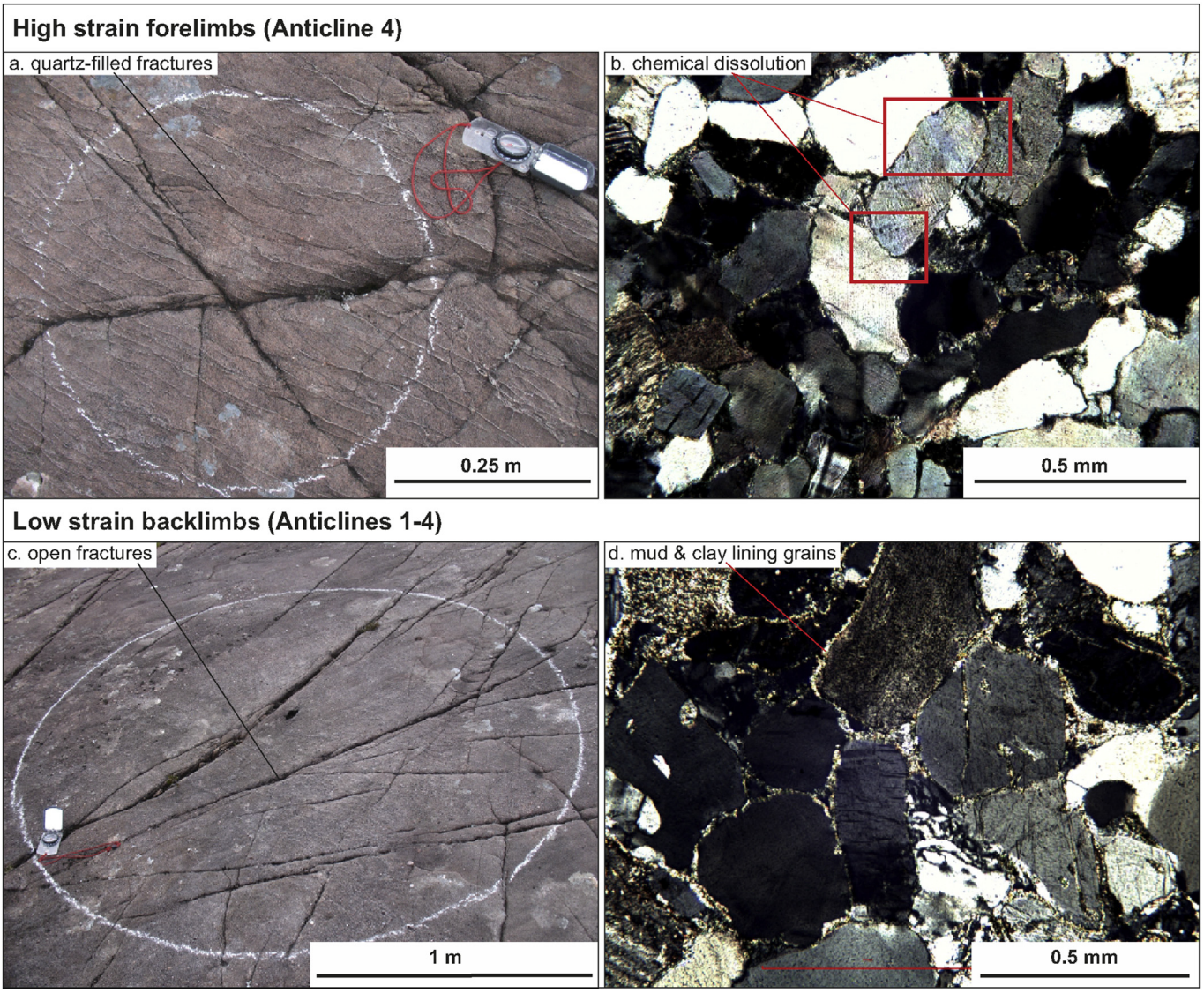

Fig. 11. a) A sampling site in the high strain forelimb of Anticline 4. Hinge-parallel fractures are short and quartz-filled. b) Thin section from the high strain forelimb of Anticline 4 showing evidence for chemical dissolution, a possible source of quartz-fill in fractures. c) A low strain back-limb sampling site, where fractures are usually long and open. d) Thin section from a low strain back-limb position, showing no evidence for chemical dissolution.

the Achnashellach Culmination has shown that fracture attributes are heterogeneous. Fracture connectivity, orientation and inferred permeability anisotropy vary significantly over short distances between adjacent sampling sites, especially in low strain backlimb regions. For example on Fig. 8, sites 7 and 8 are located 20 m apart on the same bedding surface. Site 7 has a relatively high 2D connectivity value where $C_{xy} = 81/m^2$, which might indicate high quality fractured reservoir. However, site 8, which is located only 20 m away on the same bedding surface has a C_{xy} value of $9/m^2$, which is very low and might indicate a poorly connected fractured reservoir. Similarly sites 9 and 10 (Fig. 8) have very different fracture orientations, despite being located only 45 m apart.

These observations bring into question the representativeness of data collected from well logs intersecting subsurface reservoir horizons. This issue is highlighted in Fig. 12, where well-scale circular scanlines have been digitally placed on two fracture trace maps from the study area. The circular scanline data for the well-scale circles represents the maximum data resolution that would be available from a well-log or core. Well circle 1 on Fig. 12a suggests high estimated fracture intensity, which might indicate good connectivity and therefore high fractured reservoir quality. However if that well was positioned at well circle 2 or 3, it would indicate very low estimated fracture intensity, connectivity and reservoir quality. Well circle 1 on Fig. 12b shows variable fracture orientations, which might suggest isotropic permeability. However if the well was positioned at well circles 2 or 3, data would suggest the majority of fractures were oriented NW-SE, potentially creating strong permeability anisotropy. Clearly even on the scale of these fracture trace maps, fracture attributes can vary significantly. In regions of heterogeneous fracturing, well data may therefore only be representative for the volume of rock the well directly samples. To make predictions of fractures in unsampled rock the key question is what controls fracture attribute variation and heterogeneity?

6.2. Fracture prediction

Based on a fracture orientation model by Price (1966), and strain

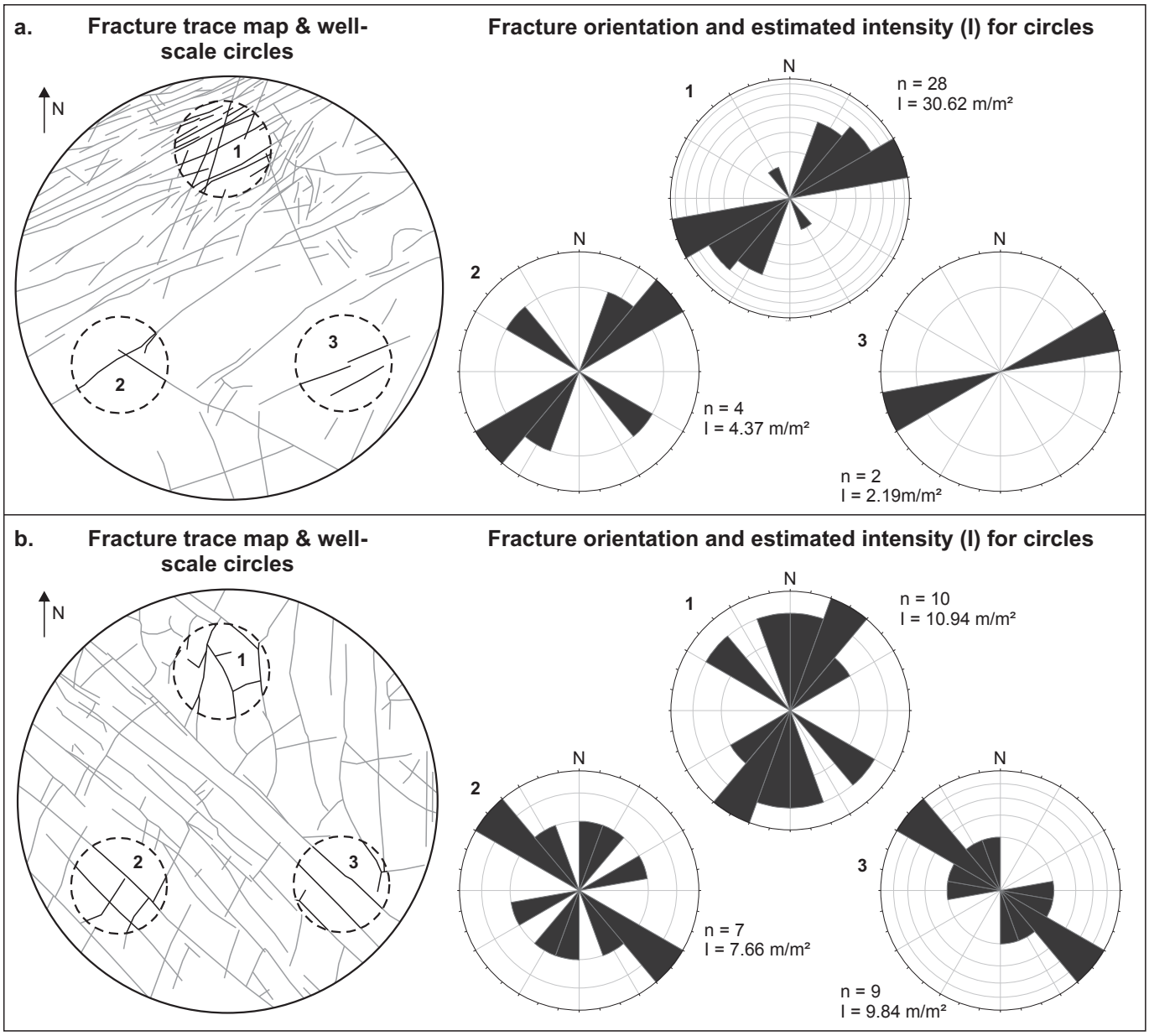

Fig. 12. Fracture trace map for two circular scanlines with a radius of 0.5 m. Three circles scaled to the approximate diameter of a well bore (9 inches, ~23 cm) have been added to each larger circle and digitised. Fracture orientations of each fracture that intersects the well-scale circles are extracted, and fracture intensity for each circle is estimated using the equation from Mauldon et al. (2001). a) For Fig. 12a the estimated fracture intensity varies from the top to the bottom of the circle. Well-scale circle 1 suggests high estimated fracture intensity (30.62 m/m^2), whereas well-scale circles 2 and 3 suggest low estimated fracture intensities (2.19–4.37 m/m^2). b) For Fig. 12b the fracture orientations vary depending on which half of the circle is sampled by the well-scale circles. Well-scale circle 1 detects near-randomly oriented fractures whereas well-scale circles 2 and 3 suggest a dominant NW-SE fracture orientation. All rose plots are area-scaled.

distribution estimated from our 3D model restoration, we predicted four main fracture sets, the estimated intensity and connectivity of which is greater in high strain regions (Fig. 5). Fracture connectivity was predicted to be high in the forelimbs of Anticlines 1 and 4, and low on the backlimbs of Anticlines 1–4. On a large scale (i.e. within the whole area covered by the 3D model, Figs. 2a and 4) our predictions are correct; combined fracture data for the entire study area show four main fracture sets whose orientations correspond with the predictions from Price (1966), and whose connectivity is generally higher in higher strain forelimb regions than lower strain backlimb regions. However, on a small scale (i.e. within individual fold structures) fracture attributes are much less predictable; fracture orientations at individual sampling sites show significant dispersion, and the orientations of dominant fracture sets are not always consistent with those predicted. Fracture orientations in the backlimbs of Anticlines 2 and 4 are dispersed, which we suggest is due to low, dispersed strain, allowing fracture orientations to vary significantly along strike despite a common deformation history. Fracture orientations in the forelimb of Anticline 4 are consistent, suggesting high, localised strain.

Fracture connectivity is also shown to vary significantly on a small scale. These variations do not appear to correspond to any changes in fold geometry or strain, and are most prominent in low strain backlimbs (e.g. see Fig. 7). We must therefore explore alternative causes for these observed connectivity fluctuations. The first explanation is that our 3D model for strain distribution (Fig. 4b)

does not have high enough resolution to show small scale strain-fluctuations. Our 3D model was constructed using cross sections spaced 300 m apart, meaning curvature and strain anomalies on a scale smaller than this cross section spacing are not incorporated. The process of 3D surface construction and smoothing would also reduce any small-scale geometric variations, meaning they too would not be incorporated into the 3D restoration and resultant strain prediction. Although modelling limitations could explain the mismatch between predicted strain and fracture connectivity, we see no clear underlying cause for such small-scale strain variations in the field area.

The variations in fracture connectivity might also relate to early-stage fracturing at low strains that might occur at the onset of deformation, before folding commenced. Since the 3D restoration only takes into account fold-related and thrust-related deformation, this early, low strain would cannot be predicted. Fractures that formed before or after compression associated with Moine thrusting could also cause fluctuations in connectivity that cannot be accounted for by variation in structural position or modelled strain. The intensities of these fracture sets observed in the foreland to the Achnashellach Culmination (i.e. in the absence of fold-associated fractures) are very low (<10 m/m^2), suggesting that they probably to not occur in great enough abundance to cause the observed connectivity variations on fold backlimbs.

An alternative explanation for such variable 2D connectivity in low strain backlimbs is a lithological control on fracture formation. Many authors have suggested lithology can significantly influence fracture intensity (e.g. Ferrill and Morris, 2008; Laubach et al., 2009; Ortega et al., 2010). Watkins et al. (2015b) determine a weak correlation between fracture intensity and grain size in the Torridon Group of the Achnashellach Culmination. Coarse grained rocks are found to have low fracture intensities, and high fracture intensities are consistently found in fine grained rocks. A weak correlation indicates that grain size is not the only lithological factor influencing fracture intensity. Studies on fractured Torridon Group sandstones and Eriboll Group quartzites elsewhere in NW Scotland suggest factors such as clay mineral cement, quartz cement and porosity all influence rock mechanical properties, and therefore the formation of fractures (Ellis et al., 2012; Laubach et al., 2014). These lithological variables are likely to influence fracture intensity in our study area. We can, however, suggest that lithology may influence fracture intensity and since estimated fracture intensity has been found to correlate to 2D connectivity (C_{xy}, Fig. 6a), it can be inferred that lithology also influences connectivity. Local variations in lithology within the Torridon Group could therefore be responsible for the anomalous fluctuations in 2D connectivity (C_{xy}) on the backlimbs of Anticlines 2 & 4 (Fig. 7a and c).

Anomalous fracture connectivity values are also found on Anticline 1 where, despite variable curvature and strain, connectivity is consistently low (<200 'x' + 'y'/m^2, Fig. 6b). An explanation for these anomalies may be found on aerial photographs where large, linear features trending roughly NNE-SSW can be seen (Fig. 13a). These features are up to 1 km long and are oriented parallel to the fold hinge. In the field they appear as grassy gullies with no exposure. Given their orientation parallel to the fold hinge and perpendicular to maximum principle stress at the time of thrusting, these features could be hinge-parallel fracture corridors that accommodate a significant proportion of strain in the forelimb

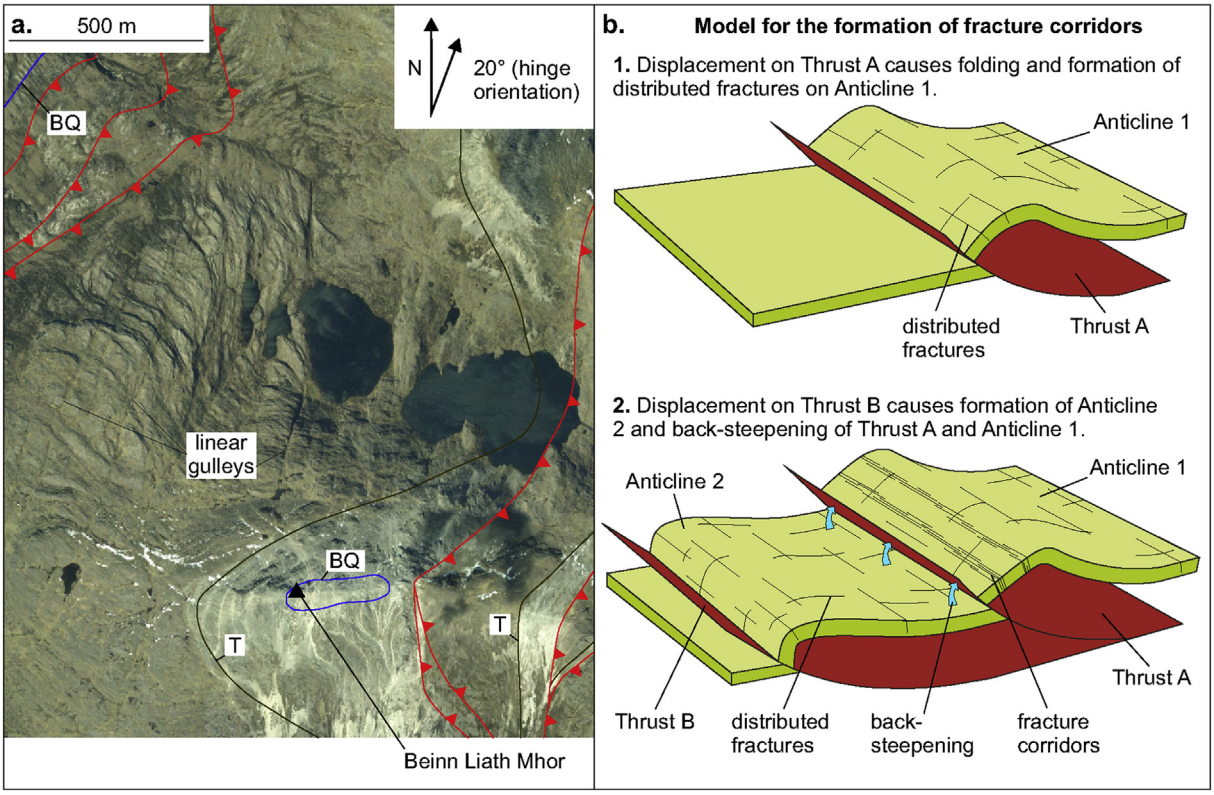

Fig. 13. a) Aerial photograph of Torridon Group sandstone outcrops on Anticline 1, showing mapped thrust traces and horizon tops for the Basal Quartzite (BQ) and Torridon Group (T) (see Fig. 2a for location of air photo). Long, linear features trending NNE-SSW are clearly visible. These may be fracture corridors that accommodated a higher proportion of strain than other parts of the fold structure. b) 3D model for the evolution of potential fracture corridors on Anticline 1. Fractures are initially distributed across Anticline 1. Subsequent deformation in the footwall of Thrust A causes backsteepening and additional strain on Anticline 1; rather than forming new distributed fractures, strain is localised in narrow zones of high intensity hinge-parallel fractures that accommodate flexure.

of Anticline 1. If this was the case, our fracture data from Anticline 1 has been taken in between these fracture corridors, in zones of relatively intact rock that has accommodated much less strain proportionally than other parts of the structure. This heterogeneous strain accommodation could explain why our fracture connectivity values are much lower than expected.

Anticline 1 has been interpreted as the oldest of the four studied structures and therefore has the longest deformation history. If these features are fracture corridors they may have formed due to concentration of deformation in hinge-parallel zones as the formation of younger folds caused back-steepening of Anticline 1's forelimb (Fig. 13b). A mechanism of back-steepening causing localisation of deformation in these linear zones might also be expected on Anticline 2, however no evidence for these features are seen on aerial photographs. Alternatively the linear features seen on Fig. 13a could be later normal faults formed after fold formation. Their orientation is parallel to normal faults seen on the north-western edge of the field area (see Fig. 2a). Because the gullies contain no exposure in the field it is not possible to determine their origin, or whether or not they do indeed contain high intensity fracturing.

6.3. *Fractured reservoir quality*

The Achnashellach Culmination was chosen as an outcrop analogue to a folded tight sandstone reservoir. Field data collected from well-exposed anticlines are used to interpret fractured reservoir quality for this outcrop analogue and summarised in Fig. 14. Regions of high curvature (fold forelimbs) were predicted to be high strain zones. Within the zones of predicted high strain, fractures have high estimated intensity and are well connected. The high curvature forelimbs have a single, dominant fracture orientation that is parallel to the fold hinge, resulting in strong predicted permeability anisotropy. Fracture characteristics are consistent along strike and on different bedding surfaces, increasing predictability. A predictable network of well-connected fractures would make an ideal fractured reservoir; however, fractures in these high curvature forelimbs are consistently quartz-filled, potentially giving very low or non-existent secondary porosity and permeability. These regions would therefore have very low fractured reservoir quality (Fig. 14).

In contrast, low curvature regions (backlimbs) were predicted to be low strain zones. Connectivity in these regions is generally lower than high curvature forelimbs; however, it can be highly variable, probably in response to varying estimated fracture intensity. Dispersed fracture orientations within these low curvature regions mean permeability should be more isotropic than high curvature forelimbs. Fracture connectivity and permeability anisotropy tend to be very inconsistent along strike and on different bedding surfaces meaning that they are unpredictable in low strain regions. If lithological variation has influenced fracture formation then these inconsistencies could relate to local changes in lithology along strike and between beds. Despite the variation in fracture attributes, most fractures are open in low curvature backlimbs, meaning they would provide more secondary porosity and permeability than the high curvature forelimbs, and therefore have higher fractured reservoir potential (Fig. 14).

Thin sections from high strain regions showed evidence for quartz grain indentation (convex and concave grain boundaries), which may be evidence for chemical dissolution. Chemical

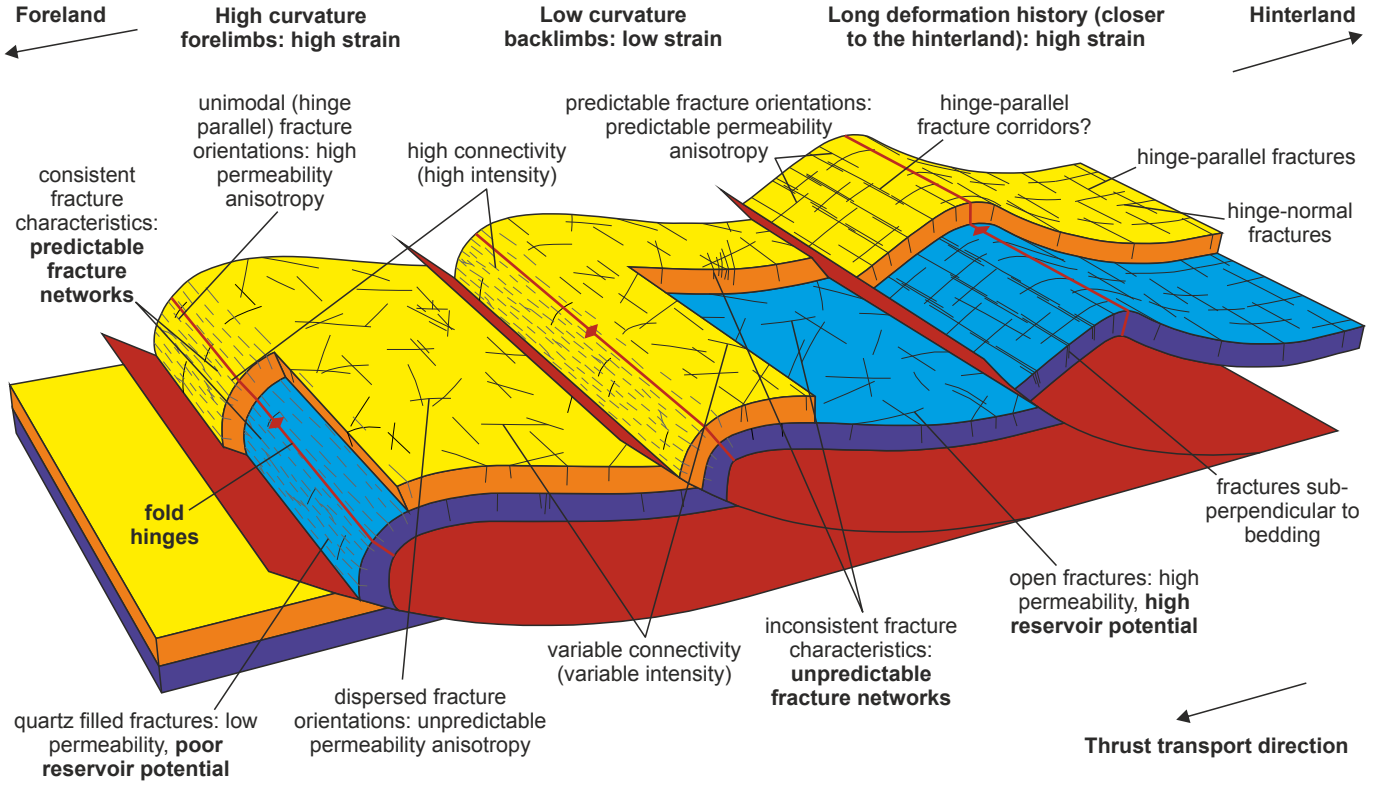

Fig. 14. Summary 3D diagram showing fracture variations at different structural positions. In high curvature regions, fractures have high connectivity and intensity, and are oriented parallel to fold hinges. Fractures are quartz-filled. In low curvature regions fractures generally have lower but highly variable connectivity and intensity and unpredictable orientations. Fractures are open. In structures with longer deformation histories, fractures are oriented either parallel or perpendicular to fold hinges, and potentially have fracture corridors that accommodate high strain.

dissolution may have occurred during thrusting-related compression, meaning quartz-was re-precipitated locally in newly-formed joints that opened as a result of folding. No evidence for chemical dissolution is seen in the low strain regions, which could explain the lack of quartz-fill in fractures at outcrop. Our observations regarding quartz-fill are in contrast to global clastic reservoirs and outcrops, where quartz cementation is pervasive, regardless of large-scale structure (Parris et al., 2003; Becker et al., 2010; Fall et al., 2014). In these cases quartz cementation in fractures does not rely on local quartz sources, such as dissolution by chemical dissolution. If chemical dissolution is not the cause of quartz fill in our study, then alternative explanations for the preferential quartz cement in high strain zones must be explored. Compositional differences within our study area may cause the lack of quartz cement in low strain zones. The mud and clay grain coating observed in thin sections from the low strain regions (Fig. 11d) may be inhibiting quartz cementation as they are, unlike the quartz grains, poor nucleation sites for quartz cement growth (Worden and Morad, 2009; Lander and Laubach, 2015). Although this is possible, detailed lithological classification has not been undertaken for our field sites.

Alternatively, the open fractures in the low strain zones of our field area could be later or earlier deformation features and do not relate to folding. A similar conclusion was made by Hennings et al. (2000), who found that folding-related fractures are preferentially developed in the higher strain plunging regions of Oil Mountain anticline, and open fractures in the backlimb are interpreted to be older, and have developed prior to folding. In our study area age-relationships between different fracture sets are very difficult to determine, with no consistent cross-cutting or abutting relationships being observed. The fracture intensities measured in the low strain regions of our study area are, however, elevated in comparison to those in the foreland to the thrust belt that have undergone a similar deformation history with the exception of folding (Watkins et al., 2015b). Because of this we conclude that the elevated fracture intensities in these low strain regions probably do relate to folding, in which case they would have been in existence at the time of quartz cementation in the high strain regions.

The difference in fracture fill throughout the study area suggests that strain may be a controlling factor, if chemical dissolution is the source of secondary quartz. Where strain is predicted to be very high, in the forelimb of Anticline 4 (Fig. 4b), we suggest chemical dissolution to be the cause of fractures being infilled with quartz (see Fig. 11). Where strain is predicted to be lower, throughout the rest of the study area (Fig. 4b), fractures remain open, possibly because no mechanism for chemical dissolution existed during deformation, or because mud and clay lining grains prevented nucleation. In this outcrop analogue, we suggest strain is responsible for both creating favourable fracture attributes that increases fractured reservoir quality and destroying secondary permeability, therefore reducing fractured reservoir potential.

The relationship between curvature, strain and fractured reservoir potential in older structures becomes more complex. We suggest structures with longer deformation histories may have accumulated significant strain during their formation, despite low curvature. The subsequent formation of folds closer to the foreland caused, in the most hinterland fold, localisation of strain in hinge-parallel fracture corridors, meaning strain is not evenly distributed. Fractures in these older structures have consistent orientations; either hinge-parallel or hinge-normal, meaning permeability anisotropy could be predictable. Fractures in these regions may have high connectivity if they are in the fracture corridors, or low connectivity if they are in intact regions in between fracture corridors. As well as being predictable, fractures appear to be open, meaning potentially high reservoir quality (Fig. 14). If the quartz cement in fractures does originate from chemical dissolution then this might mean strain in Anticline 1, although higher than backlimb regions, was not quite high enough to cause compaction and quartz dissolution. Alternatively if the lack of quartz cement in open fractures is due to lithological factors such as high clay content prohibiting quartz nucleation on fracture walls, then fractures may also remain open in Anticline 1 due to high clay and mud content.

Our inferences regarding fracture attributes of the Achnashellach Culmination suggest that, in general, fractured reservoir quality is likely to be higher in low strain regions where fractures are open and therefore have the highest relict porosity and permeability. It is not fully understood what controls fracture variations in these low strain regions; possibly because the sampling circles cover such a small percentage of the study area (circular scanlines cover only 0.00267% of the total 3D model area). Sampling a much higher outcrop area might aid in a better determination of fracture controls, however acquiring such a high sampling resolution would practically be unrealistic. In this particular example low strain regions with unexplained fracture network variations make up over 70% of fold surfaces, meaning less than 30% of the area is understood, where fracture properties are predictable.

Our suggestion that lower strain regions have higher fractured reservoir potential than high strain regions is in contrast to global examples of proven hydrocarbon reserves where wells are drilled in fold forelimbs and crests. As well as hydrocarbons accumulating in structural highs, strain is predicted to be high, corresponding to well-connected fractures in these regions. Global examples include the Apennines of Italy (Bertello et al., 2010); the Zagros (Bordenave and Hegre, 2005); the Papuan fold-thrust belt (Hill et al., 2010); the Sub-Andean fold-thrust belt (Iñigo et al., 2012); and the foothills to the Canadian Rockies (Cooper, 1992;; Hayes, 2009; Solano et al., 2010). Although estimated fracture intensity and connectivity are high in high strain forelimbs of the Achnashellach Culmination, quartz accumulation has filled fractures as much as 13 mm wide, probably diminishing permeability. This means that, unlike other global examples, the high strain regions of the Torridon Group would not be viable reservoirs, assuming the quartz cementation occurred during joint formation and widening.

7. Conclusions

Field data from the Torridon Group sandstone of the Achnashellach Culmination show that there are many factors that control how fracture attributes might vary in a fold-thrust belt. These factors include structural controls such as fold curvature, structural position, strain and length of deformation history, as well as lithological controls. In combination these many factors make the resultant fracture patterns highly heterogeneous and therefore difficult to predict. Heterogeneity in fracture patterns in the subsurface can be problematic if reservoir and seal analysis modelling is conducted based on fracture data from one dimensional well logs, limited outcrop data, or conceptual models which assume homogeneous fracture distribution. These models are likely to be oversimplified and unrepresentative of the reservoir or seal horizon.

The results from our outcrop analogue suggest that although some fracture attributes in high curvature regions may be favourable for a high quality fractured reservoir (i.e. high connectivity, consistent and predictable orientation), fracture fill is the controlling factor on secondary permeability. Fractures in high curvature regions are quartz-filled. This means the highest fractured reservoir potential would actually be in low curvature regions where, despite fracture connectivity and orientation being unpredictable, open fractures would provide secondary permeability. Additional

investigation into the influence of lithological variations on fracture intensity would need to be conducted to understand the controls on fracture formation and to improve fractured reservoir prediction.

Acknowledgements

This research was funded by a NERC CASE studentship (NERC code NE/I018166/1) in partnership with Midland Valley. Midland Valley's Move software was used for cross section construction and strain modelling. 3D Field software is acknowledged for contour map creation. Mark Cooper is thanked for constructive comments. Steven Laubach and Bill Dunne are thanked overseeing the editorial process and Magdalena Ellis Curry, Bertrand Gauthier and Arthur Lavenu are thanked for constructive reviews.

References

Barbier, M., Hamon, Y., Callot, J., Floquet, M., Daniel, J., 2012. Sedimentary and diagenetic controls on the multiscale fracturing pattern of a carbonate reservoir: the Madison Formation (Sheep Mountain, Wyoming, USA). Mar. Petrol. Geol. 29, 50–67.

Becker, S.P., Eichhubl, P., Laubach, S.E., Reed, R.M., Lander, R.H., Bodnar, R.J., 2010. A 48 m.y. history of fracture opening, temperature and fluid pressure: Cretaceous Travis Peak Formation, East Texas Basin. GSA Bull. 122 (7/8), 1081–1093.

Bergbauer, S., Pollard, D.D., 2004. A new conceptual fold-fracture model including prefolding joints, based on the Emigrant Gap anticline, Wyoming. Geol. Soc. Am. Bull. 116 (3/4), 294–307.

Bertello, F., Fantoni, R., Franciosi, R., Gatti, V., Ghielmi, M., Pugliese, A., 2010. From thrust-and-fold belt to foreland: hydrocarbon occurrences in Italy. In: Vining, B.A., Pickering, S.C. (Eds.), Petroleum Geology: from Mature Basins to New Frontiers Edited by, Proceedings of the 7th Petroleum Geology Conference. Geological Society of London, pp. 113–126.

Bond, C.E., Wightman, R., Ringrose, P.S., 2013. The influence of fracture anisotropy on CO_2 flow. Geophys. Res. Lett. 40, 1284–1289.

Bordenave, M.L., Hegre, J.A., 2005. The Influence of tectonics on the entrapment of oil in the Dezful Embayment, Zagros foldbelt, Iran. J. Petrol. Geol. 28 (4), 339–368.

Brown, S.R., Bruhn, R.L., 1998. Fluid permeability of deformable fracture networks. J. Geophys. Res. 103 (B2), 2489–2500.

Butler, R.W.H., 1982. A structural analysis of the moine thrust zone between loch Eriboll and foinaven, NW Scotland. J. Struct. Geol. 4, 19–29.

Butler, R.W.H., Coward, M.P., 1984. Geological constraints, structural evolution and the deep geology of the NW Scottish Caledonides. Tectonics 3, 347–365.

Butler, R.W.H., Matthews, S.J., Morgan, R.K., 2007. Structural evolution of the Achnashellach culmination, southern moine thrust belt; testing the duplex model. In: Ries, A.C., Butler, R.W.H., Graham, R.H. (Eds.), Deformation of the Continental Crust: the Legacy of Mike Coward, Geological Society, London, pp. 103–120. Special Publication 272.

Cooper, M., 1992. The analysis of fracture systems in subsurface thrust structures from the Foothills of the Canadian Rockies. In: McClay, K.R. (Ed.), Thrust Tectonics. Chapman & Hall, pp. 391–405.

Corbett, K., Friedman, M., Spang, J., 1987. Fracture development and mechanical stratigraphy of Austin chalk, Texas. AAPG Bull. 71 (1), 17–28.

Dutton, S.P., 1993. Influence of provenance and burial history on diagenesis of lower cretaceous frontier formation sandstones, green river basin, Wyoming. J. Sediment. Petrol. 63 (4), 665–677.

Elliott, D., Johnson, M.R.W., 1980. Structural evolution in the northern part of the moine thrust zone. Trans. R. Soc. Edinb. Earth Sci. 71, 69–96.

Ellis, M.A., Laubach, S.E., Eichhubl, P., Olson, J.E., Hargrove, P., 2012. Fracture development and diagenesis of Torridon Group Applecross Formation, near an Teallach, NW Scotland: millenia of brittle deformation resilience? J. Geol. Soc. Lond. 169, 297–310.

Fall, A., Eichhubl, P., Bodnar, R.J., Laubach, S.E., Davis, J.S., 2014. Natural hydraulic fracturing of tight-gas sandstone reservoirs, Piceance Basin, Colorado. GSA Bull. 127 (1–2), 61–75.

Ferrill, D.A., Morris, A.P., 2008. Fault zone deformation controlled by carbonate mechanical stratigraphy Balcones fault system. Tex. AAPG Bull. 92 (3), 359–380.

Florez-Niño, J.-M., Aydin, A., Mavko, G., Antonellini, M., Ayaviri, A., 2005. Fault and fracture systems in a fold and thrust belt: an example from Bolivia. AAPG Bull. 89 (4), 471–493.

Gorham, F.D., Woodland, L.A., Calender, J.F., Greer, A.R., 1979. Fractures in cretaceous rocks from selected areas of the san Juan basin, New Mexico. AAPG Bull. 63, 598–607.

Guiton, M.L.E., Sassi, W., Leroy, Y.M., Gauthier, B.D.M., 2003. Mechanical constraints on the chronology of fracture activation in folded Devonian sandstone of the western Moroccan Anti-Atlas. J. Struct. Geol. 25, 1317–1330.

Han, S., Zhang, J., Zhou, Y., Bai, S., Huang, L., Wang, C., Huang, W., 2016. Formation and accumulation of lower Jurassic tight gas sands in Kekeya area of Tuha Basin, northwestern China. J. Nat. Gas Sci. Eng. 29, 101–109.

Hanks, C.L., Lorenz, J., Teufel, L., Krumhardt, A.P., 1997. Lithologic and structural controls on natural fracture distribution and behavior within lisburne Group, Northeastern brooks range and north slope subsurface, Alaska. AAPG Bull. 81 (10), 1700–1720.

Harris, J.F., Taylor, G.L., Walper, J.L., 1960. Relation of deformational fractures in sedimentary rocks to regional and local structure. AAPG Bull. 44, 1853–1873.

Hartigan, J.A., Wong, M.A., 1979. A K-Means clustering algorithm. J. R. Stat. Soc. Ser. C Appl. Stat.) 28 (1), 100–108.

Hayes, B.J., 2009. Evolution of tight gas sandstone plays and production, western Canada sedimentary basin. Search Discov. Article 10182.

Healy, D., Rizzo, R.E., Cornwell, D.G., Farrell, N.J., Watkins, H., Timmes, N.E., Gomez-Rivas, E., Smith, M., 2016. FracPaQ: a MATLAB toolbox for the quantification of fracture patterns. J. Struct. Geol. 95, 1–16.

Hennings, P.H., Olson, J.E., Thompson, L.B., 2000. Combining outcrop data and three-dimensional structural models to characterise fractured reservoirs: an example from Wyoming. AAPG Bull. 84 (6), 830–849.

Hill, K.C., Lucas, K., Bradey, K., 2010. Structural styles in the Papuan Fold Belt, Papua New Guinea: constraints from analogue modelling. In: Goffey, G.P., Craig, J., Needham, T., Scott, R. (Eds.), Hydrocarbons in Contractional Belts. Geological Society, London, pp. 33–56. Special Publication 348.

Hooker, J.N., Laubach, S.E., Gomez, L., Marrett, R., Eichhubl, P., Diaz-Tushman, K., Pinzon, E., 2011. Fracture size, frequency and strain in the cambrian Eriboll Formation sandstones, NW Scotland. Scott. J. Geol. 47 (1), 45–56.

Hobbs, D.W., 1967. The Formation of tension joints in sedimentary rocks: an explanation. Geol. Mag. 104 (6), 550–556.

Hugman, R.H.H., Friedman, M., 1979. Effects of texture and composition on mechanical behavior of experimentally deformed carbonate rocks. AAPG Bull. 63 (9), 1478–1489.

Iñigo, J.F., Laubach, S.E., Hooker, J.N., 2012. Fracture abundance and patterns in the Subandean fold and thrust belt, Devonian Huamampampa Formation petroleum reservoirs and outcrops, Argentina and Bolivia. Mar. Petrol. Geol. 35, 201–218.

Johnson, M.R.W., Kelley, S.P., Oliver, G.J.H., Winter, D.A., 1985. Thermal effects and timing of thrusting in the Moine Thrust zone. J. Geol. Soc. Lond. 142, 863–874.

Krabbendam, M., Prave, T., Cheer, D., 2008. A fluvial origin for the Neoproterozoic morar Group, NW Scotland implications for torridon-morar Group correlation and the Grenville orogen foreland basin. J. Geol. Soc. 165, 379–394.

Krabbendam, M., Leslie, A.G., 2010. Lateral variations and linkages in thrust geometry: the traligill transverse zone, Assynt culmination, moine thrust belt, NW Scotland. In: Law, R., Butler, R.W.H., Strachan, R.A., Krabbendam, M. (Eds.), Continental Tectonics and Mountain Building: the Legacy of Peach and Horne. Geological Society, London, pp. 335–357. Special Publication 335.

Lander, R.H., Laubach, S.E., 2015. Insights into rates of fracture growth and sealing from a model for quartz cementation in fractured sandstone. GSA Bull. 127 (3–4), 516–538.

Laubach, S.E., Olson, J.E., Gale, J.F.W., 2004. Are open fractures necessarily aligned with maximum horizontal stress? Earth Planet. Sci. Lett. 222, 191–195.

Laubach, S.E., Diaz-Tushman, K., 2009. Laurentian palaeostress trajectories and ephemeral fracture permeability, cambrian Eriboll Formation sandstones west of the moine thrust zone, NW Scotland. J. Geol. Soc. Lond. 166, 349–362.

Laubach, S.E., Olson, J.E., Gross, M.R., 2009. Mechanical and fracture stratigraphy. AAPG Bull. 93 (11), 1413–1426.

Laubach, S.E., Eichhubl, P., Hargrove, P., Ellis, M.A., Hooker, J.N., 2014. Fault core and damage zone fracture attributes vary along strike owing to interaction of fracture growth, quartz accumulation, and differing sandstone composition. J. Struct. Geol. 68, 207–226.

Laubach, S.E., Fall, A., Copley, L.K., Marrett, R., Wilkins, S.J., 2016. Fracture porosity creation and persistence in a basement-involved laramide fold, upper cretaceous frontier formation, green river basin, USA. Geol. Mag. 153 (5/6), 887–910.

Lisle, 1992. Constant bed-length folding: three dimensional geometrical implications. J. Struct. Geol. 14 (2), 245–252.

Lisle, R.J., 1994. Detection of zones of abnormal strains in structures using Gaussian curvature analysis. AAPG Bull. 78, 1811–1819.

Long, J.C.S., Remer, J.S., Wilson, C.R., Witherspoon, P.A., 1982. Porous media equivalents for networks of discontinuous fractures. Water Resour. Res. 18 (3), 645–658.

Manzocchi, T., 2002. The connectivity of two-dimensional networks of spatially correlated fractures. Water Resour. Res. 38 (9), 1162–1181.

Mauldon, M., Dunne, W.M., Rohrbaugh, M.B., 2001. Circular scanlines and circular windows: new tools for characterizing the geometry of fracture traces. J. Struct. Geol. 23, 247–258.

McClay, K.R., Coward, M.P., 1981. The moine thrust zone: an overview. In: McClay, K.R., Price, N.J. (Eds.), Thrust and Nappe Tectonics, Geological Society, London, pp. 241–260. Special Publication 9.

McQuillan, 1973. Small-scale fracture density in Asmari formation of southwest Iran and its relation to bed thickness and structural setting. AAPG Bull. 57 (12), 2367–2385.

Mendum, J.R., Barber, A.J., Butler, R.W.H., Flinn, D., Goodenough, K.M., Krabbendam, M., Park, R.G., Stewart, A.D., 2009. Lewisian, Torridonian and Moine Rocks of Scotland, Geological Conservation Review Series, vol. 34. Joint Nature Conservation Committee, Peterborough.

Midland Valley Exploration Ltd, 2013. Move 2013.1. Midland Valley Exploration Ltd., Glasgow.

Midland Valley Exploration Ltd, 2014. Move 2014.1. Midland Valley Exploration Ltd.,

Glasgow.
Murray, G.H., 1968. Quantitative fracture study, sanish pool, McKenzie county, North Dakota. AAPG Bull. 52, 57–65.
Nelson, R.A., 1985. Geological Analysis of Naturally Fractured Reservoirs, second ed. Gulf Publishing, Houston, Texas.
Nelson, R.A., Serra, S., 1995. Vertical and lateral variations in fracture spacing in folded carbonate sections and its relation to locating horizontal wells. J. Can. Petrol. Technol. 34, 51–56.
Oda, M., 1986. An equivalent continuum model for coupled stress and fluid flow analysis in jointed rock masses. Water Resour. Res. 22 (13), 1845–1856.
Oda, M., Hatsuyama, Y., 1987. Numerical experiments on permeability tensor and its Application to jointed Granite at stripa mine, Sweden. J. Geophys. Res. 92 (B8), 8037–8048.
Ortega, O.J., Gale, J.F.W., Marrett, R., 2010. Quantifying diagenetic and stratigraphic controls on fracture intensity in platform carbonates: an example from the Sierra Madre Oriental, northeast Mexico. J. Struct. Geol. 32, 1943–1959.
Ozkan, A., Cumella, S., Milliken, K.L., Laubach, S.E., 2009. Prediction of lithofacies and reservoir quality using well logs, late cretaceous Williams Fork Formation, mamm creek field, piceance basin, Colorado. AAPG Bull. 95 (10), 1699–1723.
Parris, T.M., Burruss, R.C., O'Sullivan, P.B., 2003. Deformation and the timing of gas generation and migration in the eastern brooks range foothills, Arctic National wildlife refuge, Alaska. AAPG Bull. 87 (11), 1823–1846.
Peach, B.N., Horne, J., Gunn, W., Clough, C.T., Hinxman, L.W., Teall, J.J.H., 1907. The geological structure of the north-West highlands of Scotland. Memoirs Geol. Surv. G. B.
Price, N.J., 1966. Fault and Joint Development in Brittle and Semi-brittle Rocks. Pergamon, Oxford.
Provot, X., 1995. Deformation Constraints in a Mass-spring Model to Describe Rigid Cloth Behavior. Proceedings of Graphics Interface, New York, pp. 147–155.
Rainbird, R.H., Hamilton, M.A., Young, G.M., 2001. Detrital zircon geochronology and provenance of the Torridonian, NW Scotland. J. Geol. Soc. Lond. 158, 15–27.
Roberts, A.M., Holdsworth, R.E., 1999. Linking onshore and offshore structures: mesozoic extension in the Scottish Highlands. J. Geol. Soc. Lond. 156, 1061–1064.
Shackleton, J.R., Cooke, M.L., Seed, G., Gibbs, A., 2009. Three-dimensional modelling of Sant Corneli Anticline (Spain) using a hybrid-geometric/geomechanical approach. In: Conference paper AAPG Annual Convention and Exhibition, Denver, Colorado, June 7-10, 2009.
Solano, N., Zambrano, L., Aguilera, R., 2010. Cumulative gas production distribution on the Nikanassin tight gas formation, Alberta and british columbia, Canada. SPE Reserv. Eval. Eng. 14 (3), 357–376.
Stearns, D.W., 1969. Fracture as a mechanism of flow in naturally deformed layered rocks. In: Proceedings, Conference on Research in Tectonics, Geological Survey of Canada Paper 68–52.
Stewart, A.D., 2002. The Later Proterozoic Torridonian Rocks of Scotland: Their Sedimentology, Geochemistry and Origin. Geological Society, London, Memoirs, p. 24.
Strachan, R., Alsop, I., Friend, C., Miller, S., 2010. An Excursion Guide to the Moine Geology of the Northern Highlands of Scotland. Edinburgh Geological Society & Geological Society of Glasgow in associations with NMS Enterprises Ltd.
Swett, K., 1969. Interpretation of depositional and diagenetic history of Cambro-Ordovician succession of North-west Scotland. In: Kay, M. (Ed.), North Atlantic: Geology and Continental Drift, pp. 630–646. American Association of Petroleum Geologists Memoir 12.
Van De Kamp, P.C., Leake, B.E., 1997. Petrology, geochemistry and Na metasomatism of Torridon rift clastic rocks, NW Scotland. Scott. J. Geol. 33, 105–124.
Watkins, H., Bond, C.E., Butler, R.W.H., 2014. Identifying multiple detachment horizons and an evolving thrust history through cross-section restoration and appraisal in the Moine Thrust Belt, NW Scotland. J. Struct. Geol. 66, 1–10.
Watkins, H.E., 2015. Characterising and Predicting Fracture Patterns in a Sandstone Fold-and-thrust Belt. Ph.D. Thesis. University of Aberdeen.
Watkins, H., Bond, C.E., Healy, D., Butler, R.W.H., 2015a. Appraisal of fracture sampling methods and a new workflow to characterise heterogeneous fracture networks at outcrop. J. Strcut. Geol. 72, 67–82.
Watkins, H., Butler, R.W.H., Bond, C.E., Healy, D., 2015b. Influence of structural position on fracture networks in the Torridon Group, Achnashellach fold and thrust belt, NW Scotland. J. Struct. Geol. 74, 64–80.
Wennberg, O.P., Svånå, T., Azizzadeh, M., Aqrawi, A.M.M., Brockbank, P., Lyslo, K.B., Ogilvie, S., 2006. Fracture intensity vs. mechanical stratigraphy in platform top carbonates: the Aquitanian of the Asmari Formation, Khaviz Anticline, Zagros, SW Iran. Pet. Geosci. 12, 235–245.
Wennberg, O.P., Azizzadeh, M., Aqrawi, M.M., Blanc, E., Brockbank, P., Lyslo, K.B., Pickard, N., Salem, L.D., Svånå, T., 2007. The Khaviz Anticline: an outcrop analogue to giant fractured Asmari Formation reservoirs in SW Iran. In: Lonergan, L., Jolly, R.J.H., Rawnsley, K., Sanderson, D.J. (Eds.), Fractured Reservoirs. Geological Society, London, pp. 23–42. Special Publication 270.
Wilson, R.W., Holdsworth, R.E., Wild, L.E., McCaffrey, K.J.W., England, R.W., Imber, J., Strachan, R.A., 2010. Basement-influenced rifting and basin development: a reappraisal of post-Caledonian faulting patterns from the North Coast Transfer Zone, Scotland. In: Law, R., Butler, R.W.H., Strachan, R.A., Krabbendam, M. (Eds.), Continental Tectonics and Mountain Building: the Legacy of Peach and Horne. Geological Society, London, pp. 795–826. Special Publication 335.
Worden, R.H., Morad, D., 2009. Qaurtz Cementation in Oil Field Sandstones: a Review of the Key Controversies, pp. 1–20. Special Publications of the International Association of Sedimentologists 29.